COPY 1

REPORT NO. FAA-RD-74-89

INSTRUMENT LANDING SYSTEM IMPROVEMENT PROGRAM: CENTERLINE MONITOR

PATRICK H. GARRETT

ROBERT A. RONDINI

Avionics Engineering Center
Department of Electrical Engineering
Ohio University
Athens, Ohio 45701

MAY 1974

FINAL REPORT

Document is available to the public through the National Technical Information Service, Springfield, Virginia. 22151,

Prepared for

U.S. DEPARTMENT OF TRANSPORTATION
FEDERAL AVIATION ADMINISTRATION
Systems Research & Development Service
Washington, D.C. 20590

This
of the
of inf
ment
there

partment of Electrical
ics Engineering Center
System Improvement Program:
y Patrick H. Garrett and
inal report. May 1974.
74-89)
-2066-MOD 14
. Localizer, Category III.
ment Landing System.

hip
est
rn-
se

Ohio. University. Department of Electrical Engineering. Avionics Engineering Center
Instrument Landing System Improvement Program: Centerline Monitor, by Patrick H. Garrett and Robert A. Rondini. Final report. May 1974.

51 p. (RD-74-89)
Contract No. FA69WA-2066-MOD 14

1. Monitors, Centerline. 2. Localizer, Category III.
3. Localizers. 4. Instrument Landing System.
I. Garrett, Patrick H.

Technical Report Documentation Page

1. Report No. FAA-RD-74-89	2. Government Accession No.	3. Recipient's Catalog No.
4. Title and Subtitle INSTRUMENT LANDING SYSTEM IMPROVEMENT PROGRAM: CENTERLINE MONITOR		5. Report Date MAY 1974
		6. Performing Organization Code
7. Author(s) Patrick H. Garrett, Robert A. Rondini		8. Performing Organization Report No. EER 5-16
9. Performing Organization Name and Address Avionics Engineering Center, Department of Electrical Engineering, Ohio University, Athens, Ohio 45701		10. Work Unit No. (TRAIS)
		11. Contract or Grant No. FA69WA-2066-MOD 14
12. Sponsoring Agency Name and Address U.S. Department of Transportation, Federal Aviation Administration, Systems Research and Development Service, Washington D.C. 20590		13. Type of Report and Period Covered
		14. Sponsoring Agency Code
15. Supplementary Notes		

16. Abstract

Results of a study to investigate techniques for assuring Category III localizer signal integrity for roll-out guidance indicate that a surveillance method supported by sterilization of specific areas on and near the runway and quality near and far-field monitoring provide the best tradeoff between quality control and practical implementation.

A precision, portable localizer detector to provide accuracies of 0.0005 DDM needed for assessing localizer signal quality with respect to ICAO 0.005 DDM standards has been designed, built, and successfully tested.

17. Key Words: Localizer Calibrator; Category III Roll-Out; Transfer Standard; Localizer Critical Area; Precision Localizer Receiver; Path Quality Assurance; Path Derogation; Surveillance	18. Distribution Statement: Document is available to the public through the National Technical Information Service, Springfield, Virginia 22151.

19. Security Classif. (of this report)	20. Security Classif. (of this page)	21. No. of Pages	22. Price
UNCLASSIFIED	UNCLASSIFIED	51	

Form DOT F 1700.7 (8-72) Reproduction of completed page authorized

TABLE OF CONTENTS

		Page
	List of Figures	ii
	List of Tables	iv
I.	SUMMARY	1
II.	INTRODUCTION	2
III.	THEORETICAL PREDICTION OF LOCALIZER PATH DEROGATION EFFECTS	3
	3A. Diffraction of Localizer Signals around Large Aircraft	5
	3B. Reflection of Localizer Signals from Large Aircraft	9
	Specific Conclusions	11
IV.	PRECISION LOCALIZER SURVEILLANCE	12
	4A. Preliminary Investigation Results	12
	4B. System Mechanization	15
	4B1. Overview of the Implementation	15
	4B2. Nav-11 Receiver	15
	4B3. Transfer Standard Calibrator	18
	4B4. Bandpass Filter Requirements	20
	4B5. Phase Shifter	23
	4B6. Analog Computation Circuitry	25
	4B7. Analog Divider Circuit	28
	4C. Experimental Results, Errors and Recommended Improvements	33
	4C1. Experimental Results	33
	4C2. Instrumentation Errors	33
	4C3. Recommended Improvements	39
V.	RECOMMENDED PROCEDURES FOR IMPLEMENTING LOCALIZER PERFORMANCE ASSURANCE FOR CATEGORY III ROLL-OUT	42
VI.	CONCLUSIONS AND RECOMMENDATIONS	46
VII.	BIBLIOGRAPHY AND REFERENCES	47
VIII.	ACKNOWLEDGMENTS	48
IX.	APPENDICES	49

LIST OF FIGURES

Figure Number	Title	Page
Figure 3-1a. through Figure 3-1d.	Measured Course Diffraction Effects-- Heathrow Airport.	7
Figure 3-2a. through Figure 3-2c.	Theoretical Course Diffraction Effects.	8
Figure 3-3a.	Measured Effects Due to Signal Reflection-- Heathrow Airport.	10
Figure 3-3b.	Theoretical Effects Due to Signal Reflection.	10
Figure 4-1.	NAFEC Runway 13.	13
Figure 4-2.	Monitor Receiver Structure.	14
Figure 4-3.	System Timing Diagram.	14
Figure 4-4.	Precision 90/150 Hz DDM Converter.	16
Figure 4-5.	Nav-11 AGC Output versus Signal Strength at Antenna Input to Nav-11. f = 110 MHz.	17
Figure 4-6.	Transfer Standard Calibrator (Block Diagram).	19
Figure 4-7.	Transfer Standard Calibrator (Circuit Diagram).	21
Figure 4-8.	Bandpass Filter Attenuation.	22
Figure 4-9.	Precision Average Value Circuit.	25
Figure 4-10.	90/150 Amplitude Radio in Decibels.	27
Figure 4-11.	Algebraic Circuit.	28
Figure 4-12.	DDM Calculation and Display.	30
Figure 4-13a.	90/150 Converter.	31
Figure 4-13b.	Trim Pot and Test Point Locations.	32

Figure Number	Title	Page
Figure 4-14.	Precision Localizer Receiver and Calibrator--Front View.	34
Figure 4-15.	Precision Localizer Receiver and Calibrator--Side View with Cover Removed.	35
Figure 4-16.	Block Diagram of Vehicle Installation.	36
Figure 4-17.	Interior of Van.	37
Figure 4-18.	Albany Localizer Test Record.	38
Figure 4-19.	Improved Absolute Value Circuit.	41
Figure 5-1a.	A Contour Map of Peak CDI Response Caused by the Diffraction of Signals by a B-747 Aircraft Parked Perpendicular to the Centerline.	43
Figure 5-1b.	A Contour Map of Peak CDI Current Response Caused by the Diffraction of Signals by a B-747 Aircraft Parked Perpendicular to the Centerline.	44
Figure 5-1c.	A Contour Map of Peak CDI Current Response Caused by the Reflection of Signals from a B-747 Aircraft Parked Parallel to the Centerline	45

LIST OF TABLES

Table Number	Title	Page
Table 3.1.	Maximum CDI Amplitude (Peak-to-Peak).	6
Table 3.2.	Course Scalloping.	6
Table 3.3.	CDI Amplitude (Peak-to-Peak).	9
Table 4.1.	Interference Contributions.	24
Table 4.2.	Average Value Circuit Error Contributions.	26

I. SUMMARY

Results of a study to investigate techniques for assuring Category III localizer signal integrity for roll-out guidance indicate that a surveillance method supported by sterilization of specific areas on and near the runway and quality near and far-field monitoring provide the best tradeoff between quality control and practical implementation.

A precision, portable localizer detector to provide accuracies of 0.0005 DDM needed for assessing localizer signal quality with respect to ICAO 0.005 DDM standards has been designed, built, and successfully tested.

II. INTRODUCTION

The purpose of this work effort has been to investigate and experiment with techniques for monitoring and assuring Category III localizer signal integrity along the runway for aircraft roll-out operations. The work has been done under Contract DOT FA 69WA 2066 Modification 14.

Initially consideration was given to monitoring the position of the localizer on-course over the runway on a continuous basis using sample points which would provide data from which on-course position interpolation could be made. A preliminary design was completed which revealed that the implementation of such a system would be too complicated to have inherently good reliability and further, it would be expensive thus raising serious questions as to the cost/benefit aspects.

Because of the rather tight tolerances* that are placed on the localizer signal integrity by ICAO Annex 10, the factor of measuring capability including resolution and accuracy becomes important as the hardware is considered.

Specifications of some of the more recent monitoring equipment (e. g., FA 5697) in use call for .002 DDM error due to voice modulation, .001 DDM for RF level changes, .002 DDM for temperature. These would indicate that improved equipment is needed to insure a .005 DDM tolerance.

The choice of continuous versus continual monitoring was studied with a decision in favor of continual monitoring. The emphasis for roll-out guidance will be on environmental changes and these can be expected in general to be slowly varying. Exceptions such as large aircraft will be taken into account by defining certain critical areas from which these aircraft should be excluded.

The approach selected for providing the necessary performance assurance for the roll-out guidance for Category III operations is that of using a mobile van with precision receiving equipment for periodic surveillance.

---

*FN-ICAO Annex 10 in section 3.1.3.4.2 specifies that amplitudes in terms of DDM with a 95% probability be no greater than 0.005 from point B to point D where B is a point on the ILS glide slope measured along the extended runway centerline in the approach direction a distance of 3500 feet from the threshold; and D is a point 12 feet above the runway centerline and 3000 feet from the threshold in the direction of the localizer.

The rationale for this approach is that established Category III static near-field and far-field monitoring will insure integrity of the signal radiated from the array. Multipath coming from objects will be essentially constant with respect to time and would change only if the reflecting objects themselves changed positions. Major structures such as hangars and other environmental features would be slow to change with respect to time. One should note that hangar door positions might be critical and measurements would have to be made and results cataloged. Because the environment can be expected, in general, to change slowly, periodic checking of guidance should be adequate.

One exceptional case of reflecting objects must be considered, viz., the large aircraft which may occupy various locations on an airdrome and in the airspace above. Some positions of large aircraft are well known to be critical with respect to localizer signal integrity. Because of the spatial and time varying characteristics of the localizer signal perturbed by these aircraft, it is not realistic to expect interpolative techniques to adequately predict signal characteristics especially when only a very few samples could practically be taken. In view of this, the decision was made to identify worst case conditions predicted by mathematical models which had been validated with real-world measurements. Based on these, recommendations on sterilization of critical areas are made.

Work under other facets of the ILS Improvement Program at Ohio University is directed specifically toward validating the modeling techniques and then identifying the critical areas. Validation tests were originally planned as a part of this work, however, the unavailability of a jumbo aircraft in the time frame of this contract effort precluded the measurements from being made. Details of critical area analyses will be carried in progress reports in the DOT FA69WA 2066 contract series. The latest report in the series is SRDS RD (Fourth Interim, ILS Improvement Program Report).

This report contains three rather distinct items. First there is a discussion of the critical area problem involving large aircraft. Next there is the description of the precision measuring device designed specifically to give accuracy of 0.0005 DDM so that localizer signals can be examined with sufficient precision to determine if the 0.005 DDM requirement of ICAO is met. Finally a recommended procedure is given by which the

---

*There are three distinct areas of critical area work currently in progress at Ohio University. Under Modifications 5 and 11 of this DOT FA69WA 2066 contract, work has been and continues to be done on developing and refining the theoretical models and showing critical areas. Much of this work is reported in SRDS reports RD 72-71 and RD-73-137. Under Contract F33615-72-C-1396 with the U. S. Air Force work has been done in validating the models using a C-5A aircraft with the Provisional Category III system at NAFEC, Atlantic City, New Jersey. Work planned for the immediate future involves further validation using a Boeing 747. This work will be reported in SRDS report during 1974.

aforementioned techniques and equipment can be applied to provide the localizer performance assurance necessary for all weather roll-out guidance.

It should be clear that these techniques, particularly the one involving signal checks with a mobile van, could be used to minimize the requirement for certain flight checks.

In summary, the approach is to protect against short-term anomalies by sterilizing certain areas on the airdrome and volumes of airspace and against long-term variations by surveillance.

III. THEORETICAL PREDICTION OF LOCALIZER PATH DEROGATION EFFECTS

Signal derogation of the on-course localizer beam is a result of reflection from and/or diffraction around large objects. These large objects fall into two main classes: fixed objects such as buildings, towers, etc., and mobile objects which are almost exclusively comprised of the newer types of jumbo aircraft such as the Boeing 747, Douglas DC-10, and Lockheed C-5A. As a result of the strict tolerance limits for Category III operation, and in view of the narrow beam radiation patterns of the new localizer systems, the location of buildings large enough to cause path derogation effects should be restricted to areas of low signal radiation thereby minimizing the effects caused by these stationary objects.

The main path derogation effects then arise from the presence of the above mentioned "Jumbo-jet" aircraft when these aircraft are located in areas of high signal strength. Recently much work has been done in an attempt to derive mathematical models for this signal scattering and thus predict path derogation, or course bends, for a given location of a parked aircraft. Based on these predictions, certain "critical zones" are defined, these zones comprising those areas in which a parked "jumbo-jet" would produce an out-of-tolerance condition of the on-course localizer signal. Two such models have been developed and are reported in Technical Memorandum Numbers 41 and 48. One model deals with the reflection of localizer signals from large aircraft and the second deals with the diffraction of localizer signals around large aircraft. While the major criteria governing the quality of a model is the correlation between predicted results and real-world results, these two models were developed under the additional criteria of requiring a minimum of computer time to perform the necessary computations. The reflection model gives results which are in close correlation with results from other independently developed models, and with available experimental data. In the case of the diffraction model, the only data presently available to this Research Group for comparison of results is from a series of flight tests performed at Heathrow Airport, London, England. In contrast, the localizer system at Heathrow is of the Stan-37 type with a 12-element course array and the

current theoretical model is based on a 15-element V-Ring array. However, as will be further explained in section III A of this report, for locations of parked aircraft at azimuth angles of from 0° to about 3.5° from the centerline, the diffraction model gives results which are in close correlation with those obtained from the flight tests performed at Heathrow Airport.

A. Diffraction of Localizer Signals around Large Aircraft

Localizer path derogation caused by diffraction of the localizer signals around large aircraft arises when a "jumbo-jet" is positioned in such a manner that the incident signal energy strikes one side of the aircraft, is diffracted around, and reradiated from the other side of the aircraft into the approach path of incoming flights. A forthcoming SRDS report will describe a mathematical model for predicting course bends due to this diffraction effect. As noted previously, the only real-world data available at this time for comparison is from Heathrow Airport, London, England. Although the localizer system used at Heathrow is of a different type than the system used in the current theoretical model, comparisons between data were made for three carefully selected points. The majority of the course interference for aircraft parked at these three specific locations is caused by the tailfin rather than the fuselage of the aircraft. The locations are such that the azimuth angles of the tailfin from the centerline are less than 4°. At these small angles the tailfin intercepts the main course signal sidelobe, scattering a significant portion of the energy into the on-course path and thereby causing the resultant course bends. Also for angles less than 3°, the localizer course radiation patterns are standardized and thus independent of the type of localizer used at any given site.

For the three cases, the scattering aircraft, a Boeing 747, was parked perpendicular to the centerline with the tail nearest the centerline. The parameters of the three locations used for data comparison are:

Location Number	Distance From Localizer	Distance of Tail From Centerline	Azimuth To Edge of Tail
1	3960 ft.	220 ft.	3° 11'
2	6030 ft.	376 ft.	3° 34'
3	7500 ft.	275 ft.	2° 6'

Figures 3-1a, b, c, d are centerline recordings as measured at Heathrow Airport using a test van which was driven down the runway centerline at a speed of 28 miles per hour. Figures 3-1a, b, c correspond to interference caused when the Boeing 747 was parked at locations 1, 2, and 3, respectively. Figure 3-1d is a recording of the localizer signal with no interference. As can be noticed in all four of the recordings there was an error of 5 microamps in the alignment of the localizer. Also, as pointed out in the test report, "where multipath interference is present it takes the form of twin-lobe (reflection and diffraction) interference patterns". For the locations chosen, the diffraction effects would pose a serious hazard to a Category III landing in view of the large course bends introduced near the runway touchdown area.

Figures 3-2a, b, c are the theoretical results for the three locations listed above. The curves start approximately 500 feet beyond the location of the parked aircraft and extend for 4000 feet down the centerline. The two main points upon which a comparison between Figures 3-1 and 3-2 can be made are the amplitude of the course bends and the course scalloping frequency. The respective values are listed in Tables 3.1, and 3.2.

Location	Measured Value	Predicted Values	
		Static	Dynamic
1	greater than 40 μa	55 μa	46 μa
2	18 μa	21 μa	17 μa
3	35 μa	34 μa	27 μa

Table 3.1. Maximum CDI Amplitude (Peak-to-Peak).

Location	Measured	Predicted
1	3 cycles between 4300 ft. and 8500 ft.	5 cycles between 4500 and 8500
2	9 cycles between 6600 ft. and 10,600 ft.	12 cycles between 6600 and 10,600
3	7 cycles between 8000 ft. and 12,000 ft.	8 cycles between 8000 and 12,000

Table 3.2. Course Scalloping.

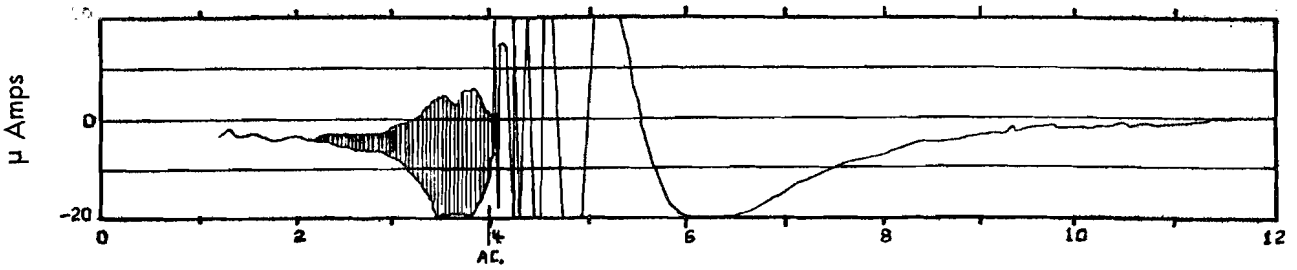

Distance From Localizer (Feet x 1000)

Figure 3-1a.

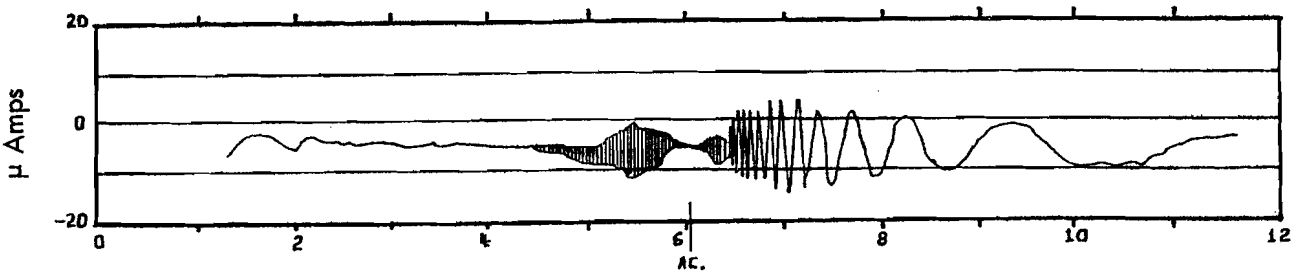

Distance From Localizer (Feet x 1000)

Figure 3-1b.

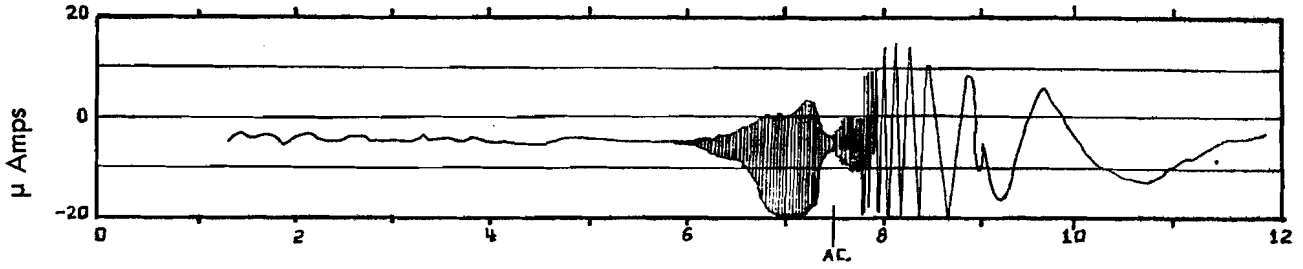

Distance From Localizer (Feet x 1000)

Figure 3-1c.

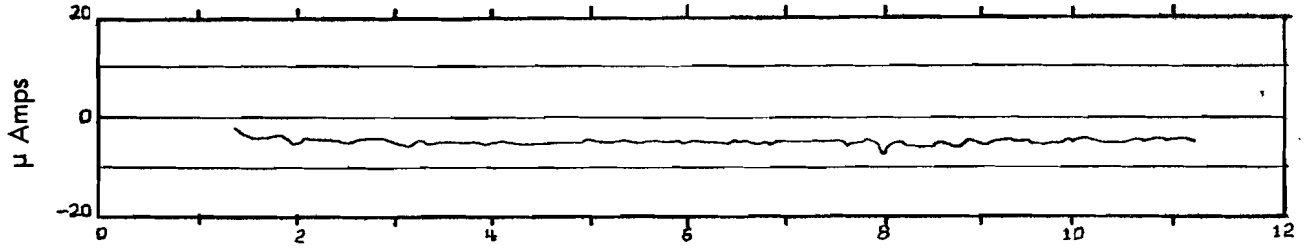

Distance From Localizer (Feet x 1000)

Figure 3-1d.

Figure 3-1a,b,c,d. Measured Course Diffraction Effects -- Heathrow Airport.

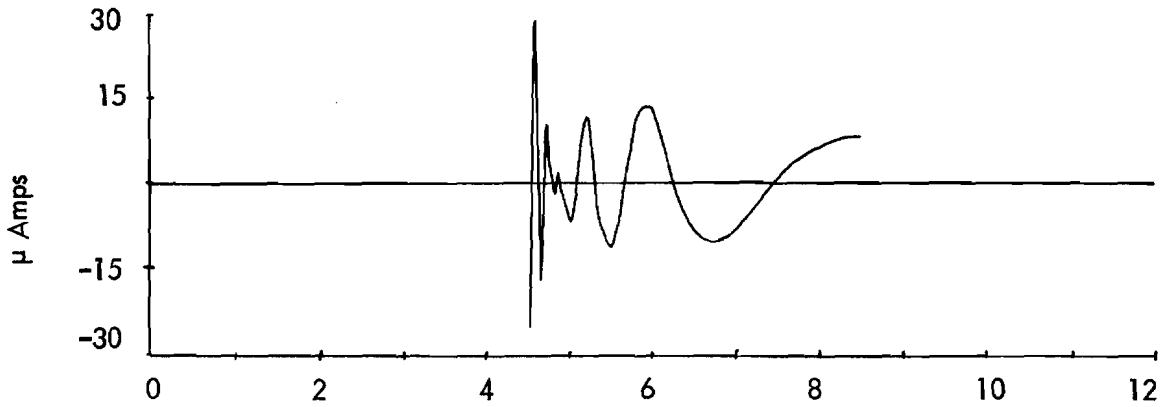

Distance From Localizer (Feet x 1000)
Figure 3-2a.

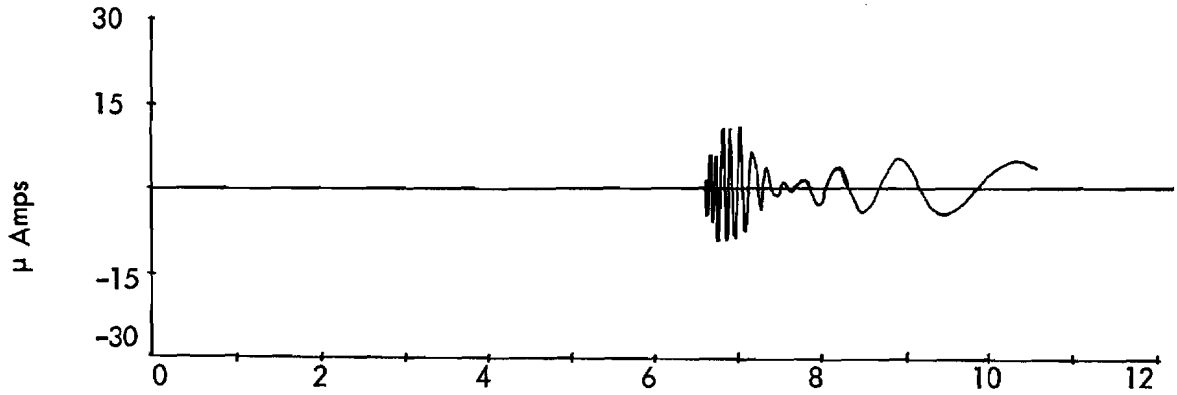

Distance From Localizer (Feet x 1000)
Figure 3-2b.

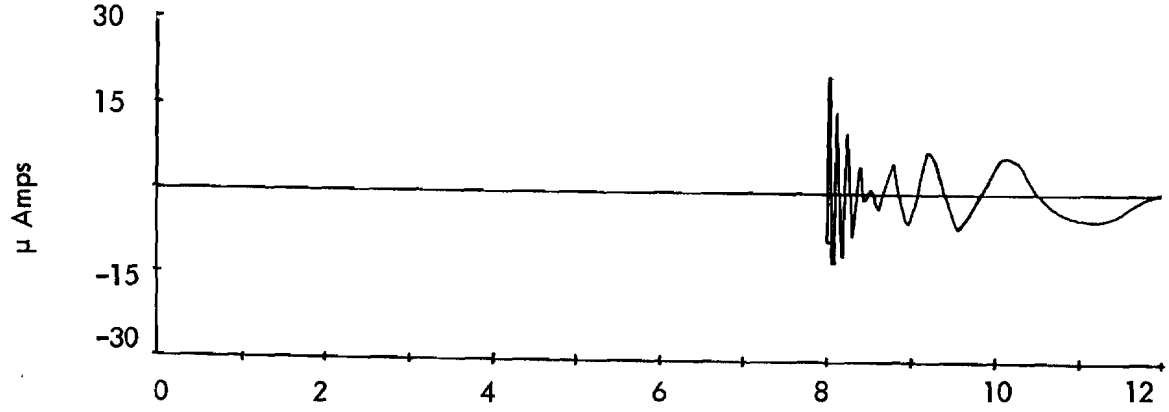

Distance From Localizer (Feet x 1000)
Figure 3-2c.

Figure 3-2a,b,c. Theoretical Course Diffraction Effects.

The dynamic CDI values are based on a receiver time constant of 0.25 seconds and a ground vehicle speed of 44 feet per second. For the three cases of interest this gives maximum peak-to-peak dynamic CDI values of .85, .80 and .79 times their respective maximum peak-to-peak static values as shown in Figures 3-2 a, b, c.

Based on the values listed in Tables 3.1 and 3.2, there appears to be good correlation between the predicted diffraction effects and the real-world diffraction effects.

B. Reflection of Localizer Signals from Large Aircraft

Localizer path derogation caused by the reflection of the localizer signal from large aircraft arises when one of these large aircraft is situated such that it reflects the off-course signal energy into the on-course approach path for incoming flights thereby giving false lateral information to the incoming flight. Technical Memorandum Number 41 describes a mathematical model for predicting course levels due to the interference of these reflected signals with the direct localizer signals. There is good correlation between the predicted results and results as computed by other independently developed models for the cases of the reflection of localizer signals from large flat objects such as hangar walls. For the case of reflection effects from a Boeing 747, the theoretical results can be compared to one set of results from the series of tests done at Heathrow Airport. The aircraft was positioned with its tail 7480 feet from the localizer, 275 feet from the centerline, and the aircraft was rotated 10° from a line parallel to the centerline, as indicated in Figure 3-3. Table 3.3 lists the measured course bend and the calculated values of the static and dynamic bends for that location. For a system time constant of $\tau = 0.25$ sec. and a ground speed of 44 feet per second for the measurement vehicle, the peak-to-peak amplitude of the dynamic CDI is .71 times the peak-to-peak value of the static CDI at the point of maximum signal derogation.

Measured Value	Theoretical Values	
	Static	Dynamic
26 μa	42 μa	30 μa

Table 3.3. CDI Amplitude (Peak-to-Peak).

Figure 3-3a shows the measured course roughness due to reflection effects, and Figure 3-3b shows the corresponding theoretical worst case results only. By worst case it is meant that the reflection model first computes only the envelope pattern of the course roughness, then the scalloping wavelength for each point is calculated from which is

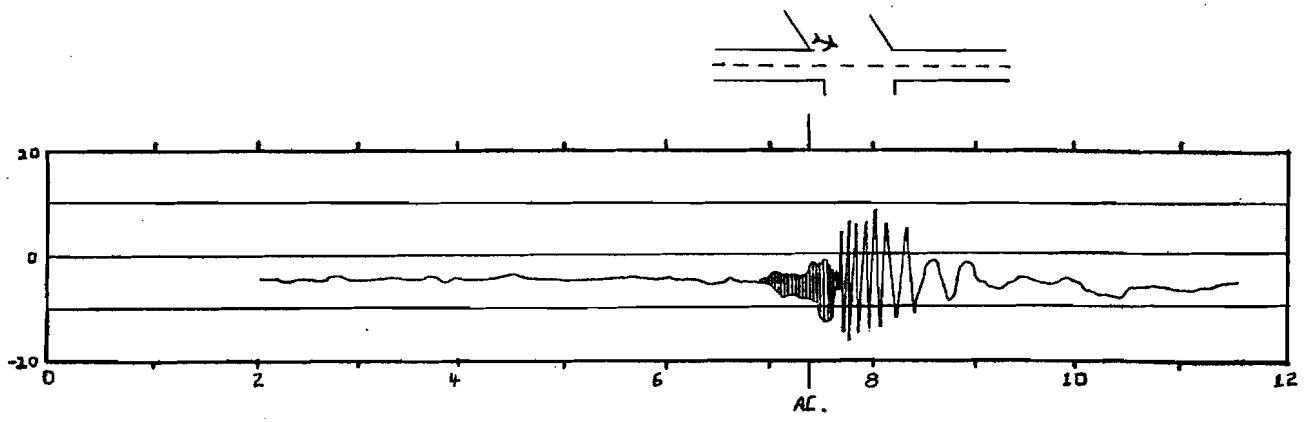

Distance from Localizer (Feet x 1000)

Figure 3-3a. Measured Effects Due to Signal Reflection--
Heathrow Airport.

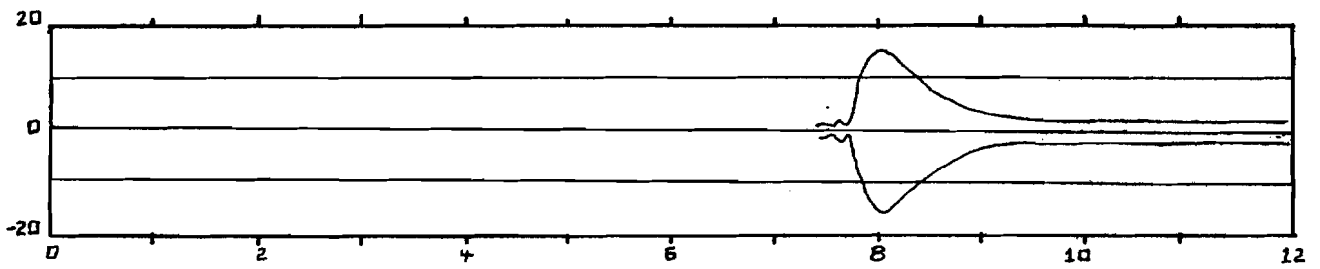

Distance from Localizer (Feet x 1000)

Figure 3-3b. Theoretical Effects Due to Signal Reflection.

obtained the static to dynamic attenuation factor. Note that the results in Figure 3-3b are dynamic CDI values. From Figure 3-3a, at maximum roughness centered around 8000 feet, the scalloping wavelength is approximately 90 feet, while at the same point the theoretical model gave a wavelength of 71 feet.

The statements made in section 3A concerning the difference of system types used to obtain the measured results and the theoretical results also apply to the comparison of results made in this section.

Specific Conclusions

The good correlation between the theoretical and measured results as listed in the previous sections illustrates the ability of the mathematical models adequately to predict course roughness arising from the scattering of signal energy by the new types of large aircraft. Based on these theoretical predictions general guidelines can be formulated to restrict these large aircraft from those critical zones on the airfield where, if present, the aircraft would produce out-of-tolerance conditions of the on-course localizer signal.

Figures 3-1 and 3-2, which depict course bending due to diffraction effects, show out-of-tolerance conditions along long portions of the centerline. While the magnitude of the bends at the threshold region of the runway are not as great as those in the vicinity of the aircraft causing the scattering, the long scalloping length of the bends in the threshold region effectively eliminates any damping of the magnitude of the course bends which might result from the landing speeds used by the incoming flights. Figure 3-3 shows that the course bending due to reflection effects is more concentrated in area along the centerline. Any out-of-tolerance conditions then would occur in the vicinity of the reflection aircraft.

The conditions depicted in Figures 3-1, 3-2, and 3-3 can easily be envisioned as happening in the daily operations of a major airfield. While a taxiing aircraft, under the direction of ground traffic controllers, would be directed to hold clear of an active runway until an incoming flight has landed, present ground traffic procedures are such as to provide only sufficient physical clearance between ground and landing traffic. To ensure safe Category III operations, the ground traffic procedures will have to be redefined to eliminate such situations, as shown in Figures 3-1, 3-2, and 3-3, where the ground traffic produces large errors in the localizer signal.

As discussed in sections 3A and 3B , since the theoretical models can predict course roughness due to signal scattering with reasonable accuracy, the models are very useful in defining appropriate critical zones for Category III operations. However, due to the complex nature of signal scattering, certain approximations must be made in order to solve the mathematics of the problem. These approximations limit the

application of the models to the specific problems for which they have been developed. Thus while these models are useful in developing general guidelines, any specific problems outside the scope of the models will require individual investigations, involving either a new mathematical development or on site measurements of the localizer signal quality.

IV. PRECISION LOCALIZER SURVEILLANCE

A. Preliminary Investigation Results

The original monitoring scheme contemplated involved the use of monitor detectors placed alongside the runway to measure the DDM gradient and thereby infer the location of zero DDM over the runway centerline. In addition to the centerline position, the width characteristics of the path would also be monitored and quantitative information obtained. Two antenna locations would be used, one bracketing Point D and the other bracketing Point E as shown by Figure 4-1, to determine the characteristics of the path. These runway side locations were chosen as more feasible than implementations placed on or in the runway for obvious reasons. Although antenna elevations of 20 feet would be desirable, airport operational requirements limit permissible heights to a few feet above ground level.

Localizer monitor receiver structures were then investigated to develop a mechanization which would provide the required accuracy. A dual-slope structure was evolved which operates in the following manner. Figure 4-2 shows the left and right antennas and a method for alternately connecting them to the receiver input. During time period t_1 the left antenna is active and the difference between the 90 Hz and 150 Hz audio levels is integrated. During period t_2 the right antenna is active and a second integration is superimposed upon the first and the resultant integrator output is described by Equation (4.1). During period t_3 the integrator output voltage is compared against upper and lower tolerance limits to effect a "go-no go" decision and then the integrator is reset. Figure 4-3 describes the system time line.

$$V_{out} = \frac{1}{RC} (V_L - V_R) \tag{4.1}$$

Two factors contributed to the conversion of the foregoing fixed monitoring scheme to a mobile implementation. The first was a rather severe requirement to accommodate the presence of aircraft and their disturbance on the electromagnetic field in the vicinity of the monitor antennas. The incidence of such perturbations was found to be in excess of 50 percent during periods of heavy airdrome traffic. The additional complexity introduced into the system to accommodate these anomalies was significant as were also the anticipated environmental problems with the low profile

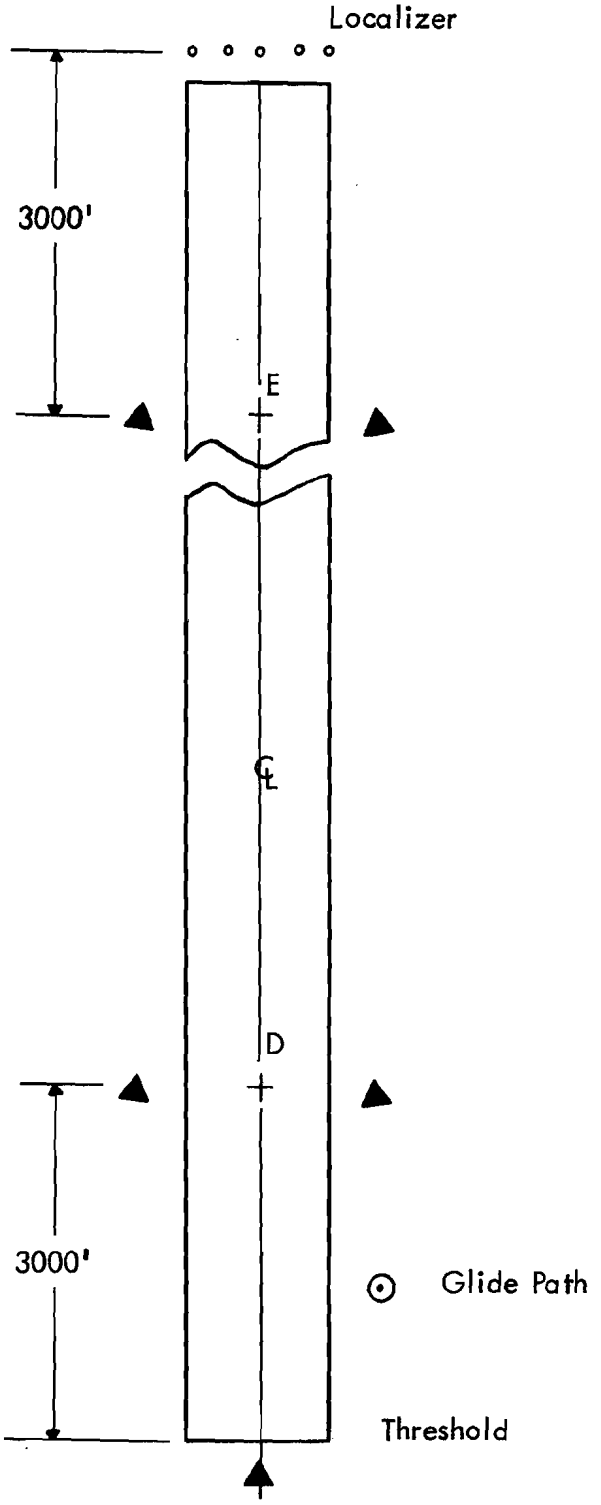

▲ Indicates Detector Point

Figure 4-1. NAFEC Runway 13

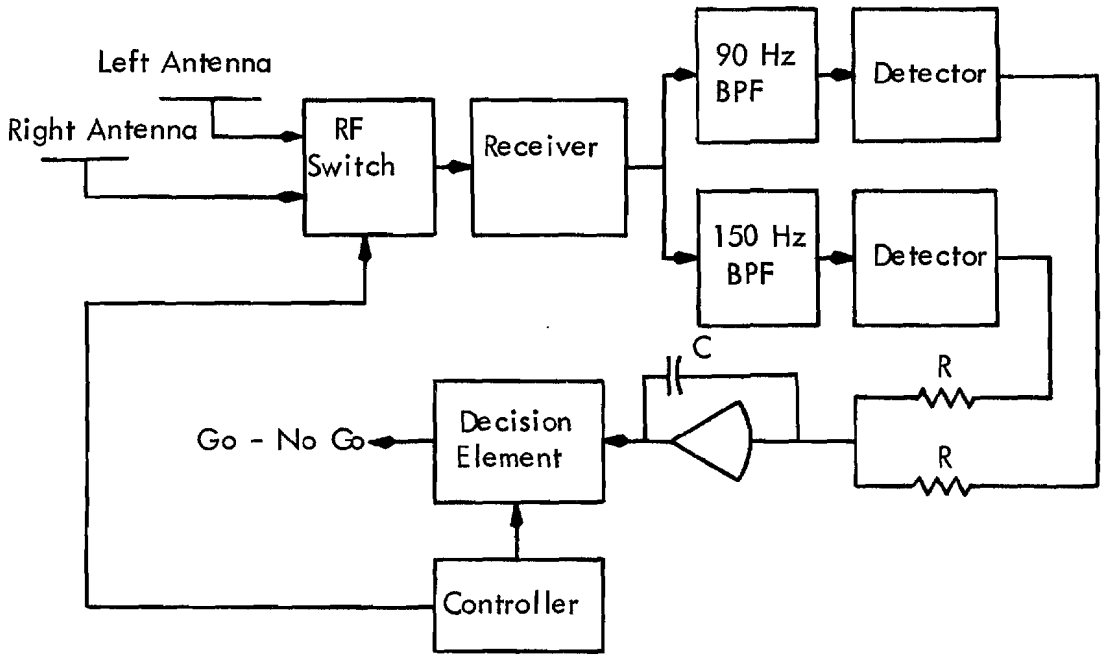

Figure 4-2. Monitor Receiver Structure.

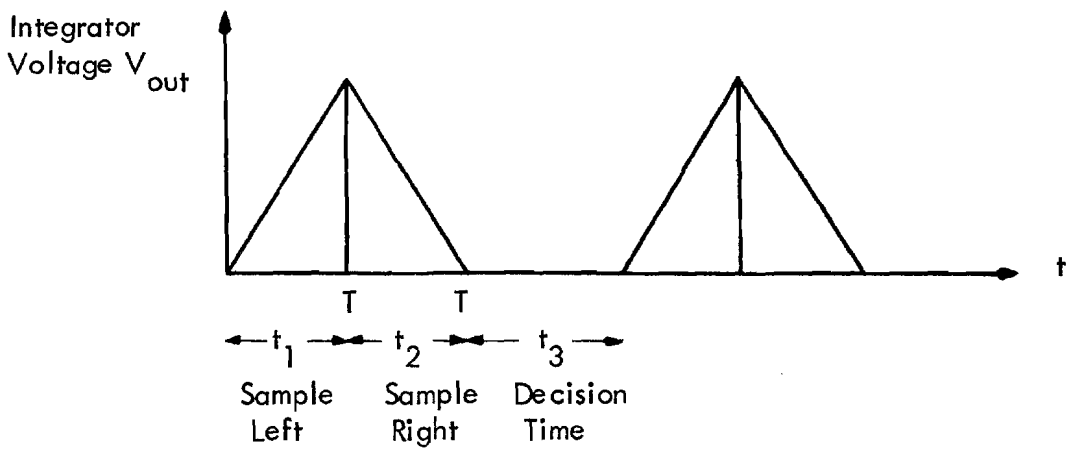

Figure 4-3. System Timing Diagram.

monitor antennas. The second factor was the development of a more flexible localizer signal monitoring system which is self-contained, mobile, less constrained by operational problems, and potentionally more useful for various localizer signal performance assurance monitoring tasks. For example, the mobility of the system to be described subsequently permits measurement of signal reflection and/or refraction effects at any point on an airport, while its precision and stability make it useful for far-field monitoring.

B. System Mechanization

1. Overview of the Implementation. A precision localizer monitor receiver has been designed and developed which permits measurements of the localizer signal to within 1 microampere worst case. The block diagram of this monitor is shown in Figure 4-4. There are five subsystems which comprise this monitor: (1) a tunable RF front-end, (2) a DDM calibrator, (3) 90 Hz and 150 Hz bandpass filters, (4) analog computation circuitry, and (5) an analog divider module which implicitly implements the DDM equation. Throughout the implementation of this device only 0.1% metal film, low temperature coefficient resistors are used. The circuitry is designed to depend upon resistance ratios rather than absolute resistance values, and the virtue of high common-mode signal rejection is utilized by constructing identical 90 Hz and 150 Hz signal channels which are operated differentially throughout the monitor. This latter feature and the implicit manner in which DDM is derived, shown by Equation (4.2), provides freedom from variations in either signal strength or receiver gain affecting DDM accuracy. Total worst-case DDM error over a 60° F temperature variation and including expected external spurious signal contributions is 0.0011 DDM, or 1.1 microamperes.

$$DDM = K \left[\frac{E150 - E90}{E150 + E90} \right] \qquad (4.2)$$

2. Nav 11 Receiver. A Narco Nav 11 localizer receiver was selected to provide the RF, tuning, and detector functions for the precision localizer monitor. This unit has a particularly good RF section, synthesizer-type superheterodyne local oscillator, and an overall state-of-the-art design. Economization in this receiver is effected in its postdetection circuitry which derives DDM information from the audio signal. This tradeoff, however, is efficient in the Nav 11 application to the precision localizer monitor design which employs high-accuracy DDM circuitry. The Nav 11 localizer receiver, therefore, provides a highly acceptable localizer receiver front-end function at an economical price.

Figure 4-5 presents a plot of the Nav 11 AGC curve of detector output voltage versus antenna terminal input voltage. The knee of this curve occurs at approximately 20 microvolts input signal. The saturation region of this AGC curve has a satisfactorily flat characteristic which enhances the already high common-mode signal rejection of

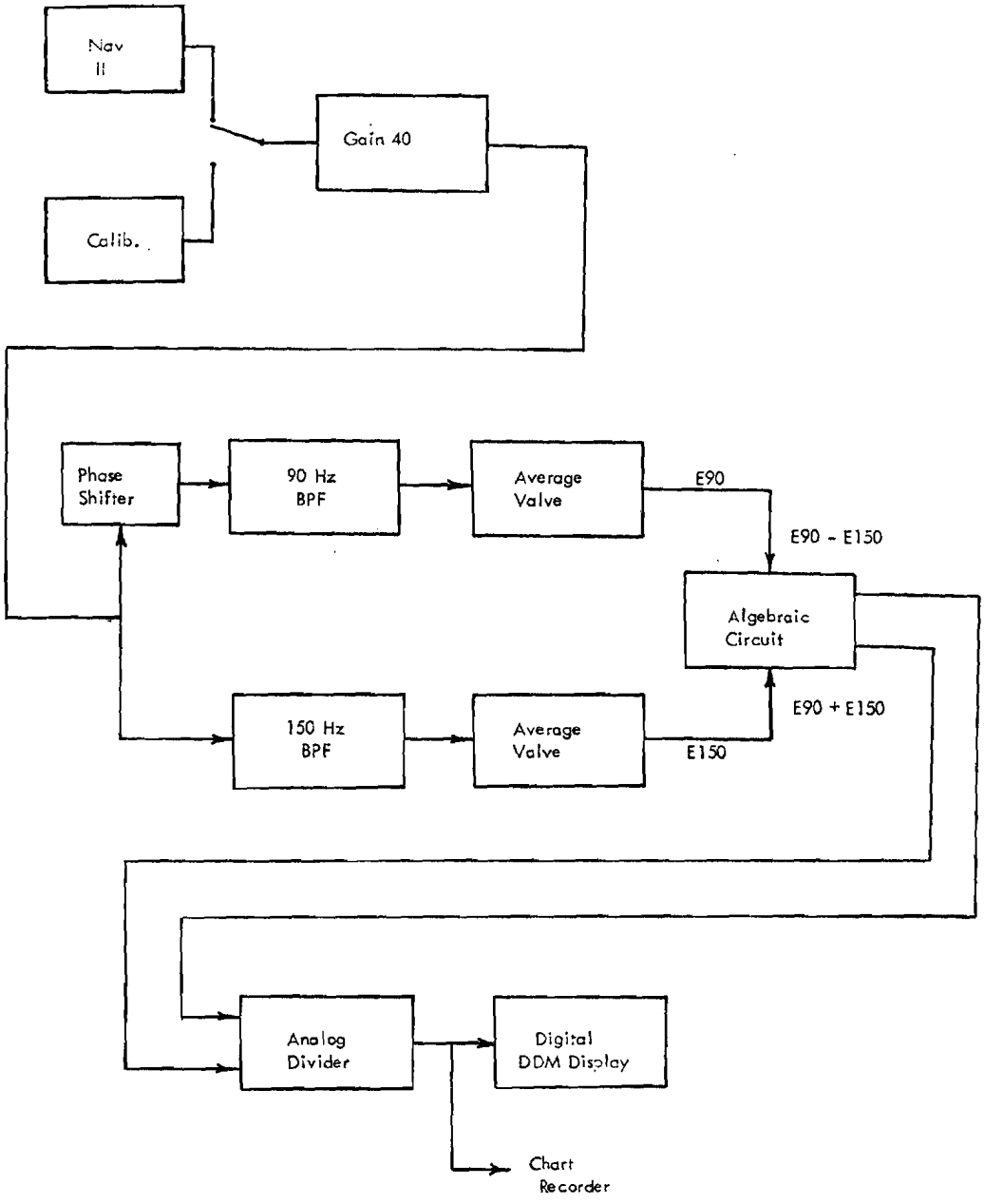

Figure 4-4. Precision 90/150 Hz DDM Converter.

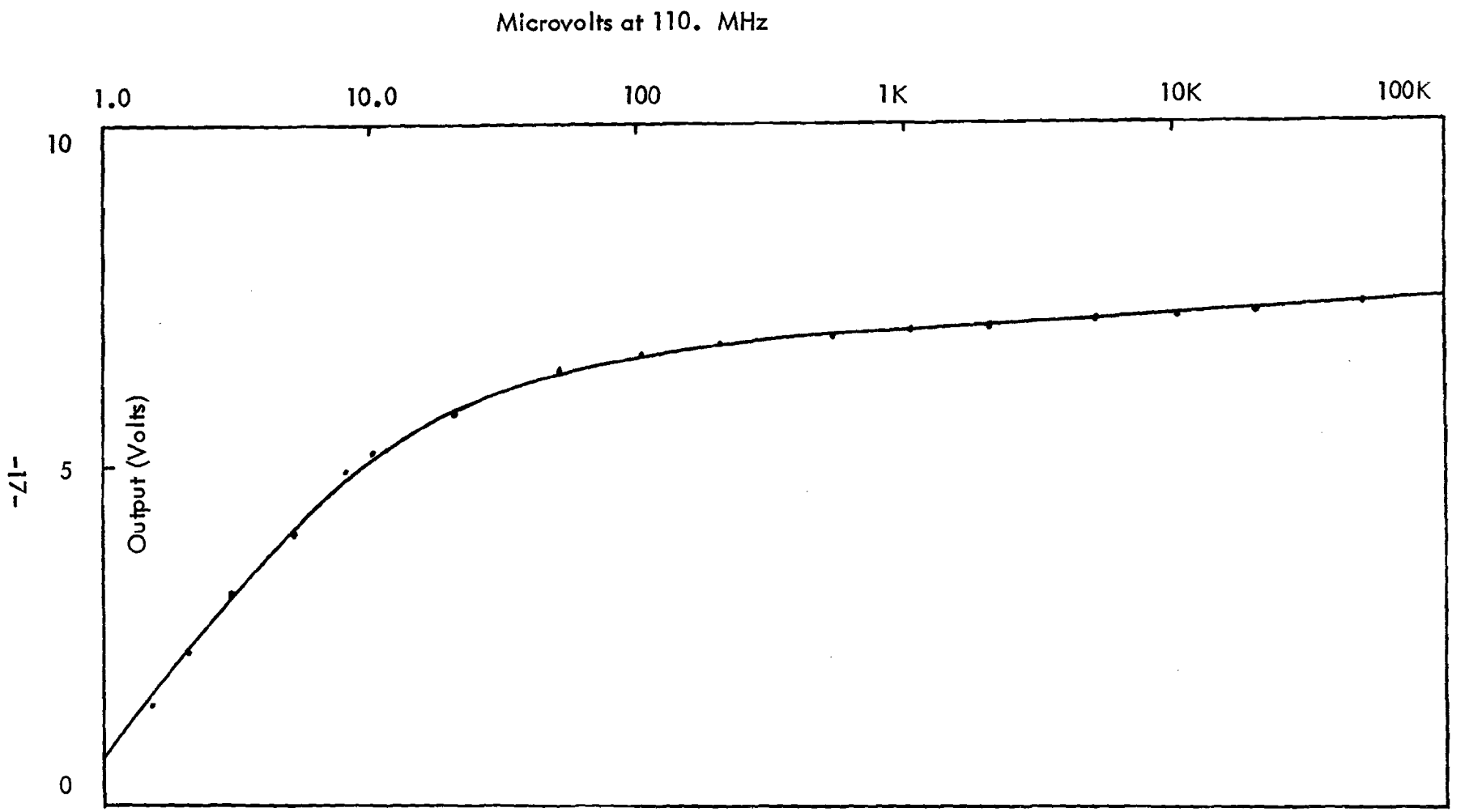

Figure 4-5. Nav 11 AGC Output versus Signal Strength at Antenna Input to Nav 11. f = 110 MHz.

the precision monitor DDM circuitry. ICAO Annex 10, which specifies localizer field strength for Category III facility performance, requires minimums of 100 microvolts per meter at 10 nautical miles and 200 microvolts per meter at the runway threshold. These field-strength conditions produce less than 0.1 volt variation in the Nav 11 detector output voltage which is further rejected by a factor of 0.005 common-mode attenuation. The resultant effect on the output DDM is typically less than 0.1%. Other pertinent Nav 11 specifications are described as follows:

Frequency Range:	108.00 to 117.95 MHz (200 channels)
Sensitivity:	1.5 μvolt nominal/2.0 μvolt maximum for 6 DB (S + N)/N ratio. 2.5 μvolt maximum for full flag
Selectivity:	50 DB down at $f_c \pm 80$ KHz
AGC Flatness:	1 DB maximum from 50 μvolts to 10k μvolts
Spurious and Image Rejection:	Exceeds requirements of RCTA Document DO-139
Environmental:	-20°C to +71°C 95% relative humidity

3. Transfer Standard Calibrator. A built-in calibrator is included in the precision localizer monitor to permit field calibration of the receiver circuitry at 0.0 DDM and ±0.090 DDM (4DB). This calibrator is tracable to a Boonton ILS calibration test set and, therefore, serves as a transfer standard to provide quality assurance of experimental measurements. The Boonton test set is a Model 211-A crystal monitored r-f signal generator. The audio components of the signal are obtained from a Collins Radio Company Type 479 S-3 signal generator using a mechanical modulator to generate the 90-150 cycle audio tones. This specific test set was last calibrated on March 20, 1973 at which time the test set "was found to meet its published operating specifications".* A copy of the Certificate of Calibration is included in this report as Appendix I.

With reference to Figure 4-6, an 18 KHz free-running multi-vibrator oscillator is temperature compensated to insure a frequency stability of 0.1% from 0° to + 55°C. The oscillator output is divided by 20 and then directed to parallel divide-by-six and divide-by-ten divider chains. These divider outputs, which are implemented with TTL JK flip-flops, are 150 Hz and 90 Hz square waves, respectively. The stability

*See Appendix I.

and accuracy of this calibrator is a function of amplitude stability rather than frequency stability. Accordingly, the square-wave outputs of the two divider chains are applied to symmetrical hard limiters which provide a consistently accurate amplitude level that is principally a function of the 0.02% regulated power supplies.

In operation, the amplitude-stable 90 Hz and 150 Hz square-wave signals are linearly combined in a resistive Y-network in three switch-selectable combinations to provide the 0 DDM and ± 0.090 DDM calibration signals. A series attenuator then reduces the amplitude of this composite signal to 0.2 volts RMS to match the level of the Nav 11 receiver envelope detector output. If the Fourier series of this composite

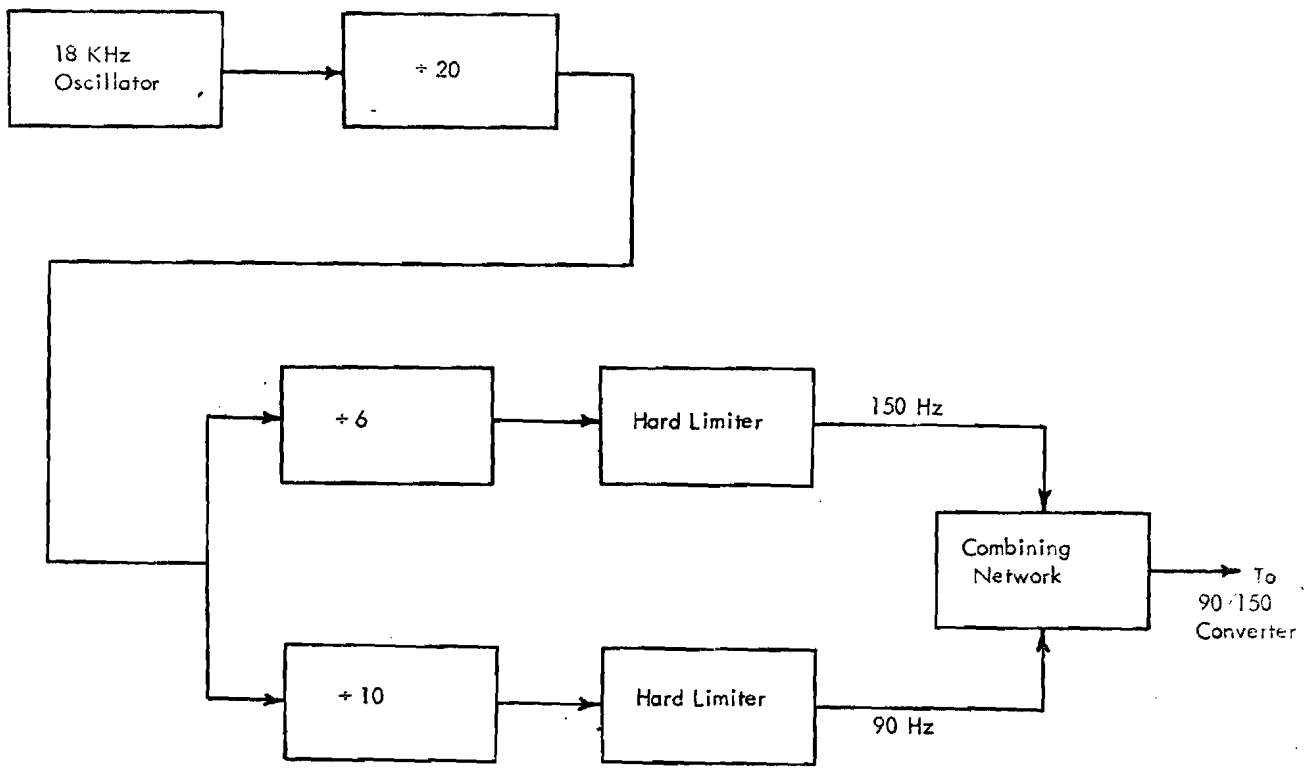

Figure 4-6. Transfer Standard Calibrator (Block Diagram).

signal is examined, both the 90 Hz and 150 Hz signals are individually defined by the odd component expansion of Equation (4.3)

$$F(t) = \frac{4V_{max}}{\pi} \sin wt + \frac{4V_{max}}{3\pi} \sin 3\,wt + \frac{4V_{max}}{5\pi} \sin 5\,wt + \ldots \qquad (4.3)$$

Application of the composite calibration signal to the Q = 15, 90 Hz and 150 Hz bandpass filters, described subsequently, permits the fundamental to pass unattenuated. The third harmonic encounters 100 DB attenuation, the fifth harmonic 120 DB attenuation, and higher-order terms even greater rejection. Therefore, accurate, stable, and very pure sinusoidal 90 Hz and 150 Hz calibration signals are provided by this transfer standard which is austere in both cost and complexity. Figure 4-7 presents the circuit diagram of this subsystem.

4. Bandpass Filter Requirements. In addition to the 90 Hz and 150 Hz course information present in the composite localizer signal, small amounts of undesired line spectra, principally 60 Hz, 120 Hz, and 180 Hz, are also typically present as well as even more diminished amounts of higher harmonics. All of these unwanted signals are present in the localizer as a result of either modulation or transmitter imperfections discussed below. Typical amounts of these three principal line spectra in the composite signal are taken as 4%. The 60 Hz signal is a modulation component which is attributable to the power line frequency. The 120 Hz signal is contributed by imperfect transmitter power supply filtering. The 180 Hz modulation component is a function of the second harmonic of the 90 Hz signal. Of these three interfering signals, 180 Hz generates the largest error in the localizer DDM reading. This is not due to a larger amplitude of 180 Hz signal, but rather to the geometric dissymmetry characteristic of bandpass filters. This is examined in greater detail in the example below.

With reference to Figure 4-8, the dashed bandpass filter characteristic curves are the measured results for a Collins 51 R3 localizer receiver. It is desirable to utilize identical Q values for both the 90 Hz and 150 Hz receiver bandpass filters. This is so that incremental changes identically affecting either the signals or the filters, such as transmitter line power transients and/or temperature effects perturbing the filter center frequencies, will result in identical gain and phase changes in both signals. The advantage of this is the preservation of the localizer receiver common-mode signal rejection introduced in Section B1 and described in detail in Section B6. Use of identical Q values for each filter, however, results in diminishing stopband attenuation with increasing frequency. Consider now the 60 Hz and 180 Hz interfering signals, which are both 30 Hz away from their respective bandpass-filter center frequencies of, respectively,

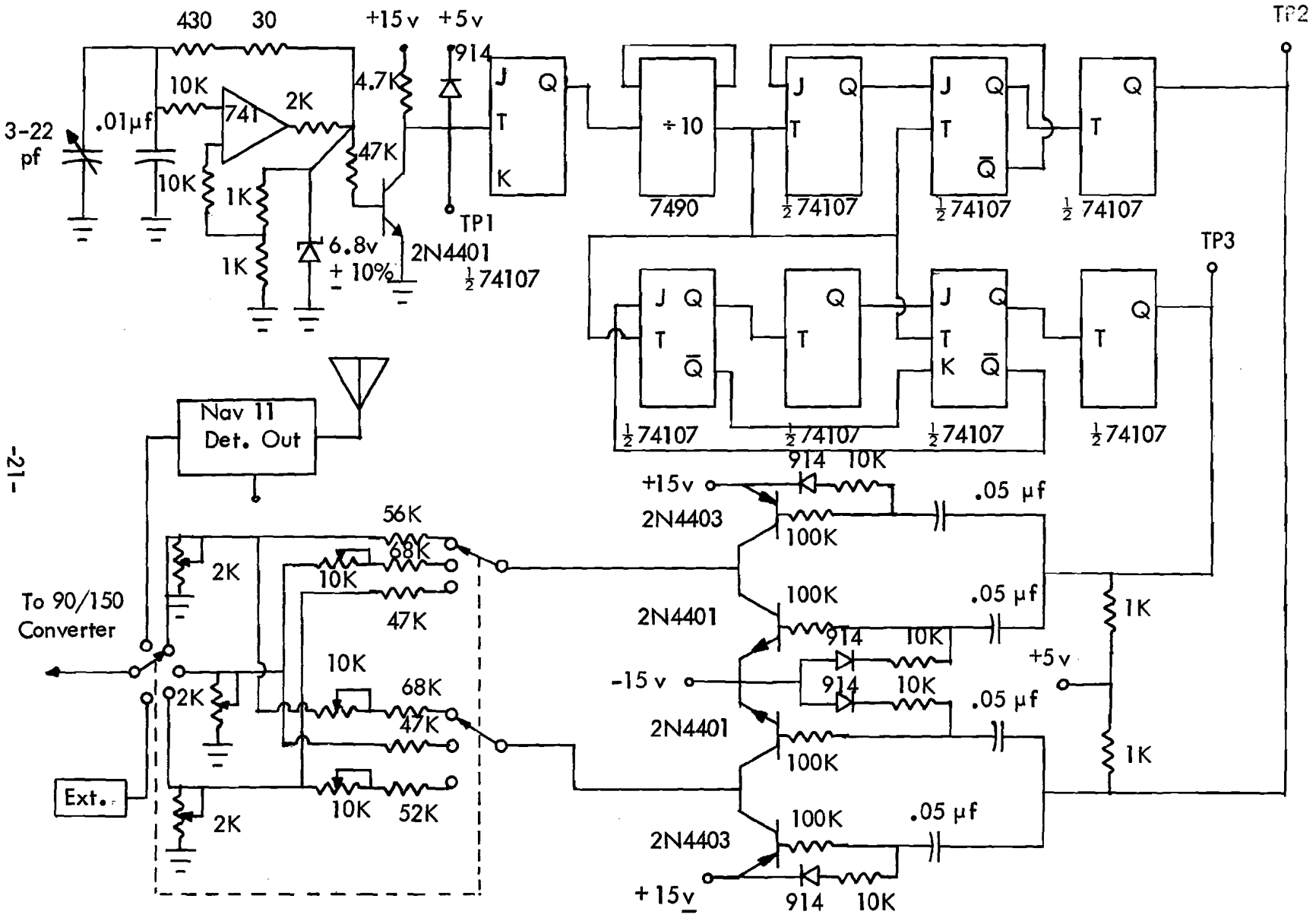

Figure 4-7. Transfer Standard Calibrator (Circuit Diagram).

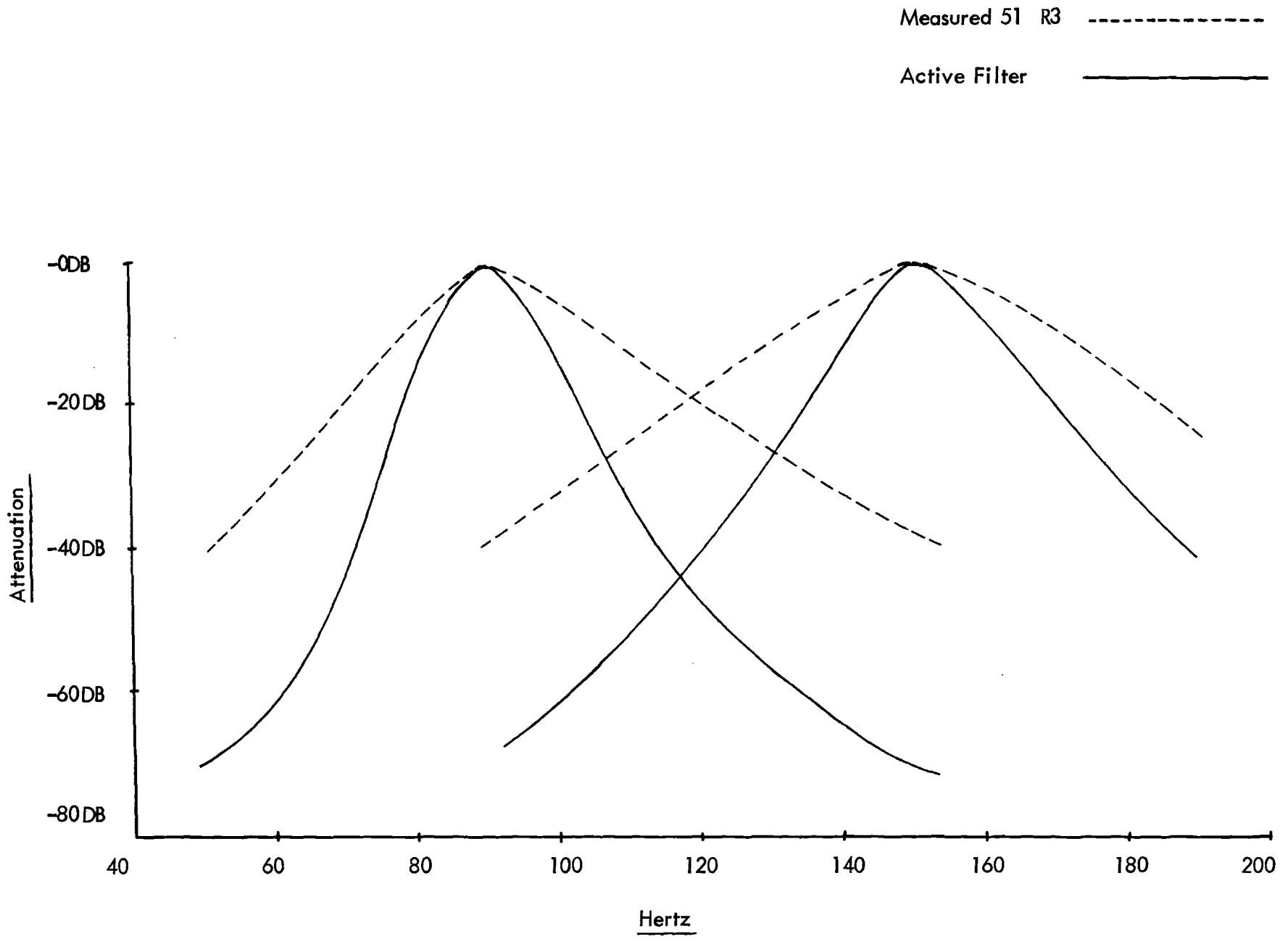

Figure 4-8. Bandpass Filter Attenuation

90 Hz and 150 Hz. For the Collins 51 R3 receiver, 30 DB of 60 Hz attenuation is achieved, but only 15 DB of 180 Hz rejection as a result of this geometric dissymmetry characteristic.

Approximately 18 DB rejection is presented by both 51 R3 bandpass filters to the 120 Hz signal. Therefore, the 120 Hz contribution to both the 90 Hz and 150 Hz channels is approximately equal resulting in a diminished effect on DDM accuracy. Also, approximately 40 DB rejection is presented to both the 150 Hz localizer signal by the 90 Hz filter, and to the 90 Hz localizer signal by the 150 Hz filter. For on-course conditions, or zero DDM, these alternate channel signal contributions are approximately equal resulting in a diminished effect on DDM accuracy. For off-course conditions, however, the alternate channel signal contributions are dissimilar and error producing due to the different 90 Hz and 150 Hz amplitude values. Having examined filter considerations for the localizer signal and its typical attendent interference, receiver filter requirements are now derived which specify the required shape factors to achieve a desired DDM measurement accuracy.

A tradeoff analysis was undertaken to determine the effect on DDM measurement accuracy due to the aforementioned interference contributions versus their attenuation by the bandpass filters for specific shape factors. Expected interference levels of four percent were assumed and DDM measurement errors then evaluated for specific attenuation values at the principal interfering frequencies of 60 Hz, 120 Hz, and 180 Hz. Table 4.1 presents a tabulation of the results denoting the bandpass filter attenuation values necessary to achieve a typical DDM error on the order of 0.1% of the full-scale 0.155 DDM value, or 0.00018 DDM. The solid curves of Figure 4-8 depict the passband/stopband attenuation values corresponding to the values tabulated in Table 4.1. In arriving at the desired filter characteristic, problems associated with the physical implementation of the bandpass filters also had to be considered which added additional complexity to the analysis. Chebyshev, Butterworth, Elliptical, Thomson, and Papoulis filter types were considered in modern active filter realizations to meet the required bandpass/bandstop requirements. The specifics of the bandpass filters used in the prototype monitor are discussed in Section C along with recommended improvements.

5. Phase Shifter. A phase shifting circuit in series with the 90 Hz bandpass filter was included to account for differences in the phase response of the 90 Hz and 150 Hz filters. This phase difference arises from the design of the filters which, according to the manufacturers, are "optimized for linear response (constant delay)".* The phase shifter compensates for the different delay times of the 90 and 150 Hz filters.

---

* Active Filters Catalog, LI-209A, Burr-Brown Research Corporation, August 1972.

	0 DDM	0.01 DDM	0.05 DDM	0.155 DDM
4% of 60 Hz in 90 Hz for 63 DB rejection	5.10×10^{-6}	4.95×10^{-6}	4.34×10^{-6}	2.60×10^{-6}
150 Hz in 90 Hz 90 Hz in 150 Hz for 70 DB rejection	0.0	0.0	8.6×10^{-8}	7.90×10^{-9}
4% of 120 Hz in 90 Hz and 150 Hz with 47 DB and 40 DB rejection, respectively	3.98×10^{-5}	4.30×10^{-5}	5.38×10^{-5}	7.60×10^{-5}
4% of 180 Hz in 150 Hz for 34 DB rejection	1.40×10^{-4}	1.39×10^{-4}	1.22×10^{-4}	7.40×10^{-5}

Table 4.1. Interference Contributions.

6. Analog Computation Circuitry. The precision localizer monitor has average value followed by algebraic matrix circuits interposed between the 90 Hz and 150 Hz bandpass filters and the divider module which implicitly implements the DDM calculation. The identical average value circuits following the two bandpass filters obtain the absolute value of the respective 90 Hz and 150 Hz signals and then converts these quantities to average DC values. Figure 4-9 shows the implementation of one average value circuit which is a precision operational amplifier full-wave rectifier followed by a low-pass active filter with a cutoff frequency of 1.59 Hz. The circuit of Figure 4-9 is optimized to provide the required performance with a minimum component count. However, it is known that a larger component count will provide increased accuracy which will be a definite topic in any follow-on effort directed

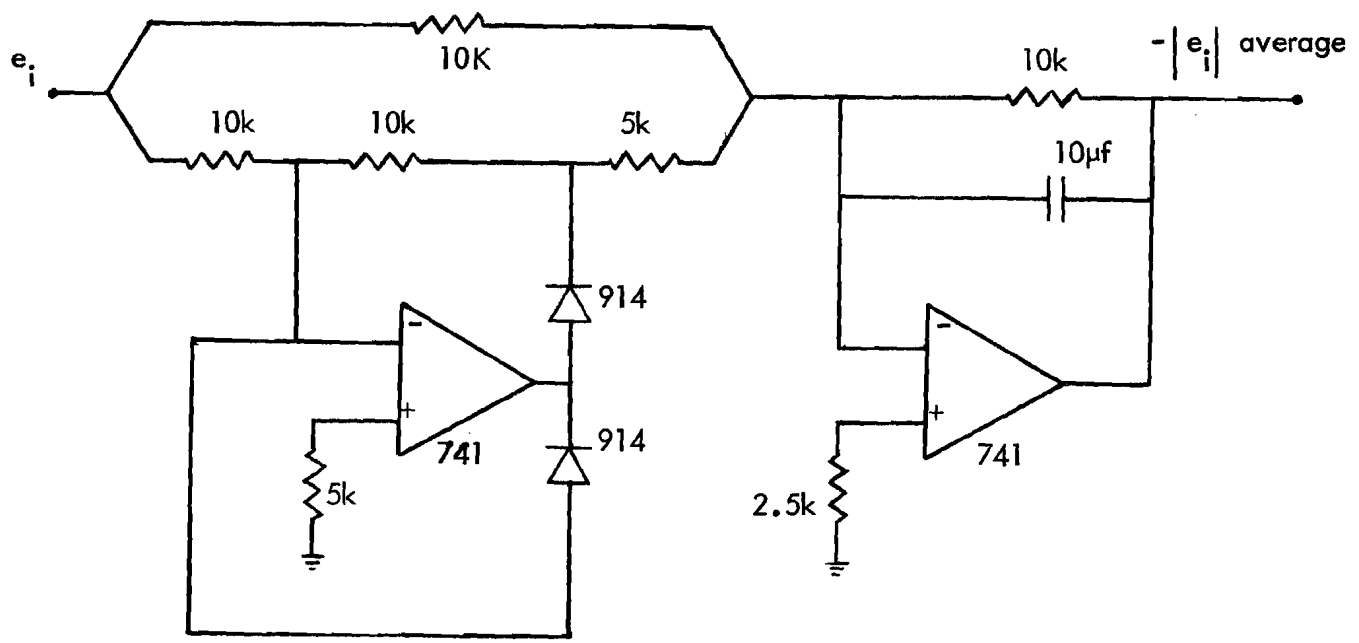

Figure 4-9. Precision Average Value Circuit.

toward product improvement. An analysis of the average value circuit errors follows.

The Fourier expansion of a full-wave rectified sinusoidal signal may be expressed as follows for the significant first three terms

$$V(w) = \frac{2}{\pi} Vm + \frac{4Vm}{3\pi} \cos 2wt + \frac{4Vm}{15\pi} \cos 4wt \qquad (4.4)$$

A single-pole RC low-pass active filter having a -3DB cutoff frequency of 1.59 Hz and a rolloff of 20 DB per decade is utilized to average these terms. Table 4.2 presents a compact tabulation of the essential parameters.

Parameter	Amplitude Values	Percentage of DC Component Amplitude	LPF Response	
			Numeric	DB
DC Component	0.6366Vm	100	1.0	0.0
2nd Harmonic	0.4244Vm	66.66	8.833×10^{-3}	-41.15
4th Harmonic	0.0849Vm	13.33	4.40×10^{-3}	-47.13

Table 4.2. Average Value Circuit Error Contributions

As shown in Table 4.2, the outputs of the average value circuits for both the 90 Hz and 150 Hz signals consist of essentially constant DC components, the magnitudes of which are proportional to the strengths of the 90 Hz and 150 Hz signals respectively.

The algebraic circuit was mechanized with a pair of operational amplifiers to provide the sum and difference of the 90 Hz and 150 Hz average value signals for the analog divider circuit. An inverting summer provides the divisor signal and a differential amplifier provides the dividend signal. The circuit shown in Figure 4-11 is optimized to provide the required performance with a minimum component count. All of the analog computation circuitry was implemented with premium active devices and 0.1% metal film resistors. Further, and as illustrated by Figure 4-11, the circuitry is configured to depend upon the accuracy of the passive devices where feasible, such as resistor ratios, in order to minimize error contributions from the anomalous behavior of the active devices.

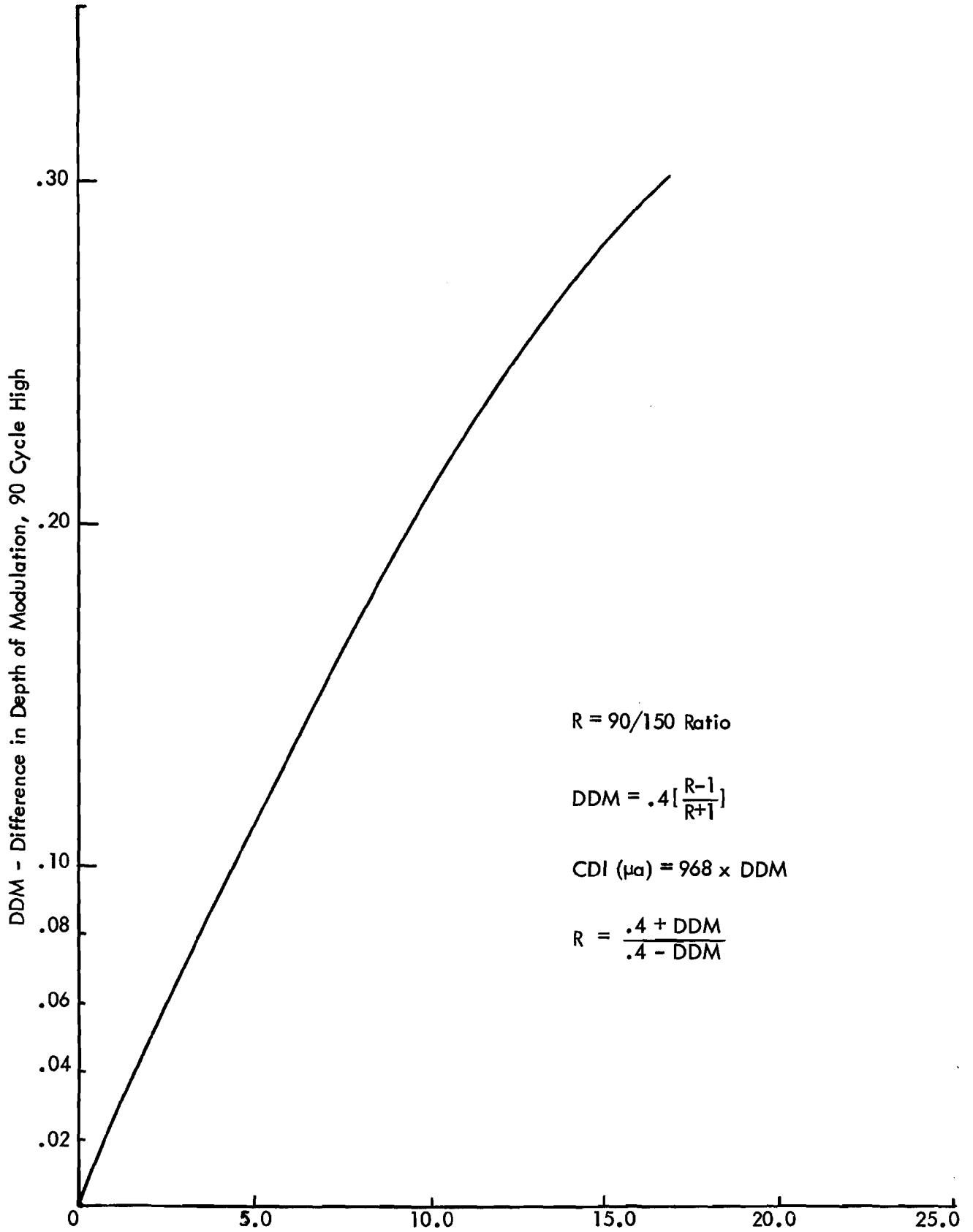

Figure 4-10. 90/150 Amplitude Ratio in Decibels.

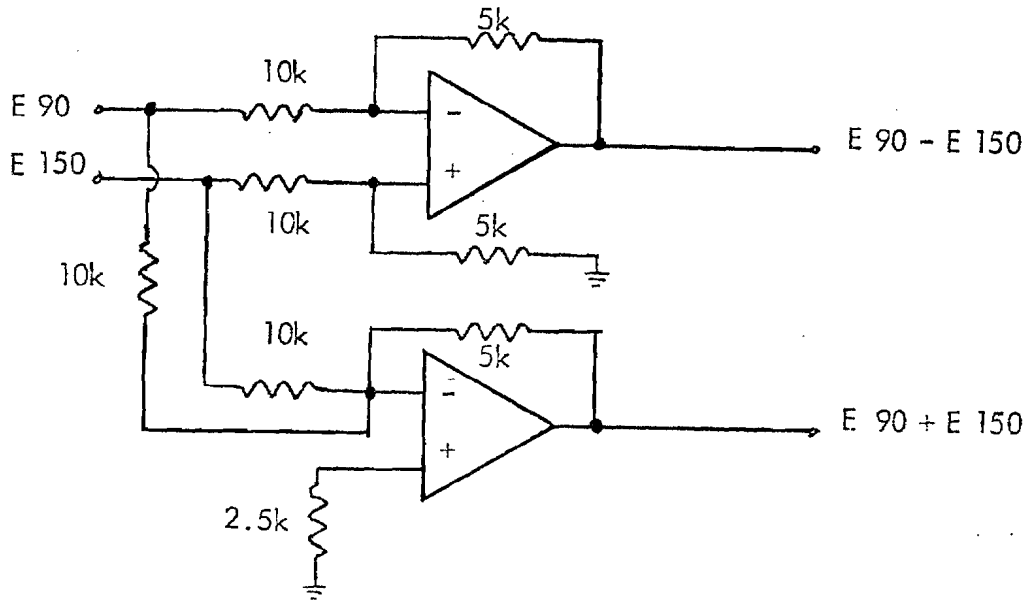

Figure 4-11. Algebraic Circuit.

7. Analog Divider Circuit. By implicitly implementing the DDM equation as described by Equation (4.2), the previously described and desirable receiver common-mode error rejection characteristics are realized. The efficient and accurate implementation of this equation is facilitated by the recently introduced 0.5% accuracy division module offered by Intronics, Incorporated, Newton, Massachusetts. This device, Model 211, is particularly useful for the mechanization at hand because it is a two-quadrant divider having a transfer function defined by Equation (4.6)

$$Eo = \frac{\pm 10\ N}{D} \qquad (4.6)$$

where $N = E\ 90 - E\ 150$ and $D = E\ 90 + E\ 150$

Figure 4-12 presents the circuit for the DDM calculation and its display. The high performance Analog Devices Model 2003 digital display has a resolution of ± 0.1 microampere, or 0.0001 DDM. Specifications for this display are described on the accompanying data sheet. Figure 4-13 is the circuit diagram for the complete precision localizer monitor exclusive of the calibration circuit, which is described by Figure 4-7 of Section B 3.

DIGITAL PANEL METERS
AD2002, AD2003

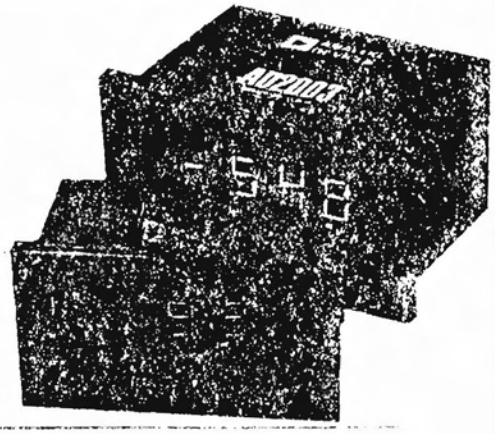

SPECIFICATION SUMMARY (Typical @ +25°C and 5VDC unless otherwise noted)

	AD2002 2½ Digit, Unipolar	AD2003 3½ Digit Differential
Display		
Number of Digits (Data Digits + 100% overrange)	2½	3½
Type	Numitron	Numitron
Overload Indication	Dashes	Dashes
Decimal Points	Selectable at Input	Selectable at Input
Filament Test	Yes	Yes
Input		
Type	Single Ended	Differential
Zero	Automatic	Automatic
Polarity	Unipolar	Bipolar
Full Scale Range	0 to +1.99V	0 to ±199.9mV
Bias Current	70nA typ./250nA max.	3nA typ./7nA max.
Impedance	>100MΩ (10k ohms in overload)	>100MΩ
Overvoltage Protection without Damage	±50V Sustained	±50V Sustained
Accuracy		
Maximum Error of Reading	0.5% ±1 Digit	0.05% ±1 Digit
Resolution	10mV	0.1mV
Temperature Range Operating	0°C to +60°C	0°C to +60°C
Temperature Coefficient	1/20 digit/°C	±50ppm/°C
Speed		
Internal Conversions/Sec	4	5
External Conversions/Sec	DP Option Up to 200	Up to 16
Hold & Read on Command	DP Option	Standard
Interface Signals (DTL/TTL Compatible)		
Inputs		
Externally Triggerable	DP Option	Standard
External Hold	DP Option	Standard
Outputs		
BCD Digits	DP Option	Standard, Latched
Overrange Signal	DP Option	Standard, Latched
Overload Signal	DP Option	Standard, Latched
Status Signal	DP Option	Standard
Polarity Signal	User Programmable	Standard, Latched
Size	5"W x 1.8"H x 1.5"D	3"W x 1.8"H x 2"D
Normal Mode Rejection		
Without Filter at 50–60Hz	Requires Filter	>40dB
Common Mode Rejection		
DC–1kHz with 1k Unbalance	Not Applicable	>80dB
Common Mode Voltage	Not Applicable	±2.5V
Power +5VDC		
Regulated ±5% (Converter)	250mA	250mA
Unregulated ±10% (Display)	500mA	750mA
Warm Up to Rated Accuracy	Essentially None	Essentially None
Adjustments	Range Potentiometer	Range Potentiometer
Price	AD2002 / AD2002/DP	
(1–9)	$75. / $83.	$140.
(100's)	$50. / $55.	$93.

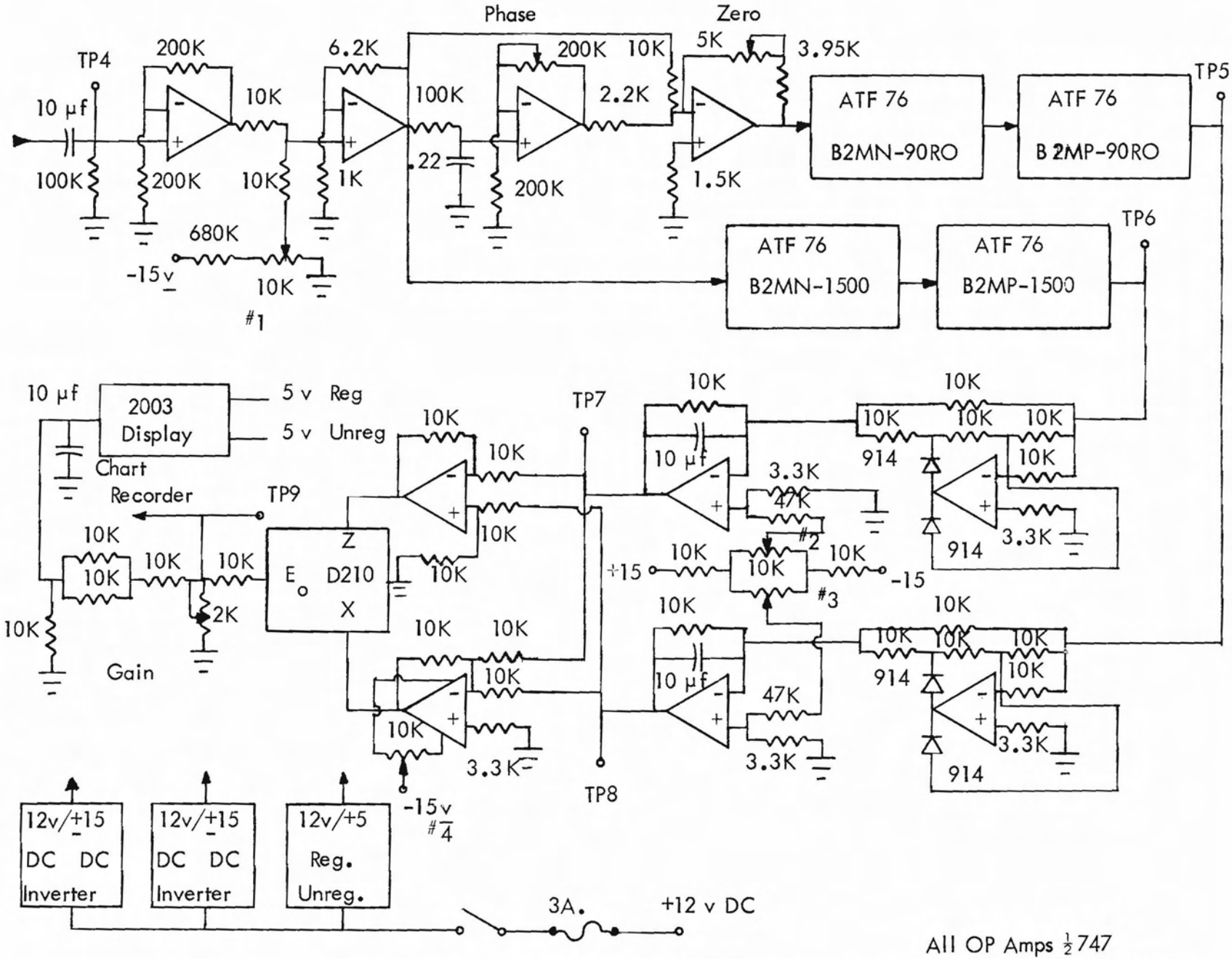

All OP Amps ½ 747
10K are 0.1% Tolerance

Figure 4-13a. 90/150 Converter.

C. Experimental Results, Errors and Recommended Improvements

1. Experimental Results. The finalized prototype precision localizer monitor, described by the circuit diagrams of Figure 4-7 and 4-13 and the foregoing circuit descriptions, is shown pictorally by Figures 4-14 and 4-15. A Ford truck van was outfitted with a rams-horn localizer antenna and a 12 VDC to 120 VAC inverter to furnish primary power. An electric odometer takeoff was fabricated and inserted into the speedometer linkage which provides a 500 millivolt ramp for each quarter mile traversed by the van. Figure 4-16 describes this van installation in block diagram fashion.

Figure 4-17 shows a dual-channel Honeywell recorder adjacent to the precision localizer receiver with the interior van view. Not shown are the heterodyne voltmeter for obtaining field-strength measurements, voice communications equipment, and power supplies. The ramp trace on the strip-chart recorder is the odometer-derived ramp signal which corresponds to linear distance traversed by the vehicle. This information is used to pin point the exact position along a runway that an event of interest occurred. Each ramp corresponds to one-quarter of a statute mile with resolution to 20 feet.

Figure 4-18 presents a compressed record of the test localizer signal over the 4000 ft. runway at Albany, Ohio. A peak localizer deviation of 15 microamperes is apparent at approximately one half mile down this runway. Other signal irregularities are observed to exist at the far end of this runway. Significant is the fact that these irregularities repeat well in successive records on this runway. Also noted on this recording is signal strength which was observed to vary from 60 microvolts at the runway threshold, to 850 microvolts at the runway far end. This signal was measured by a heterodyne voltmeter across the 50-ohm input of the receiver.

2. Instrumentation Errors. Instrumentation errors associated with the precision localizer monitor, illustrated in block diagram fashion in Figure 4-4, essentially may be lumped into four subsystems. These are: (1) the calibrator circuit, (2) the 90 Hz and 150 Hz band filters, (3) the analog computation circuitry, and (4) the DDM computation divider module. Throughout the design and implementation of this prototype instrument good engineering practice was observed and only premium component parts utilized, including 0.1% metal film, low temperature coefficient resistors. Table 4.3 presents these errors in compact form.

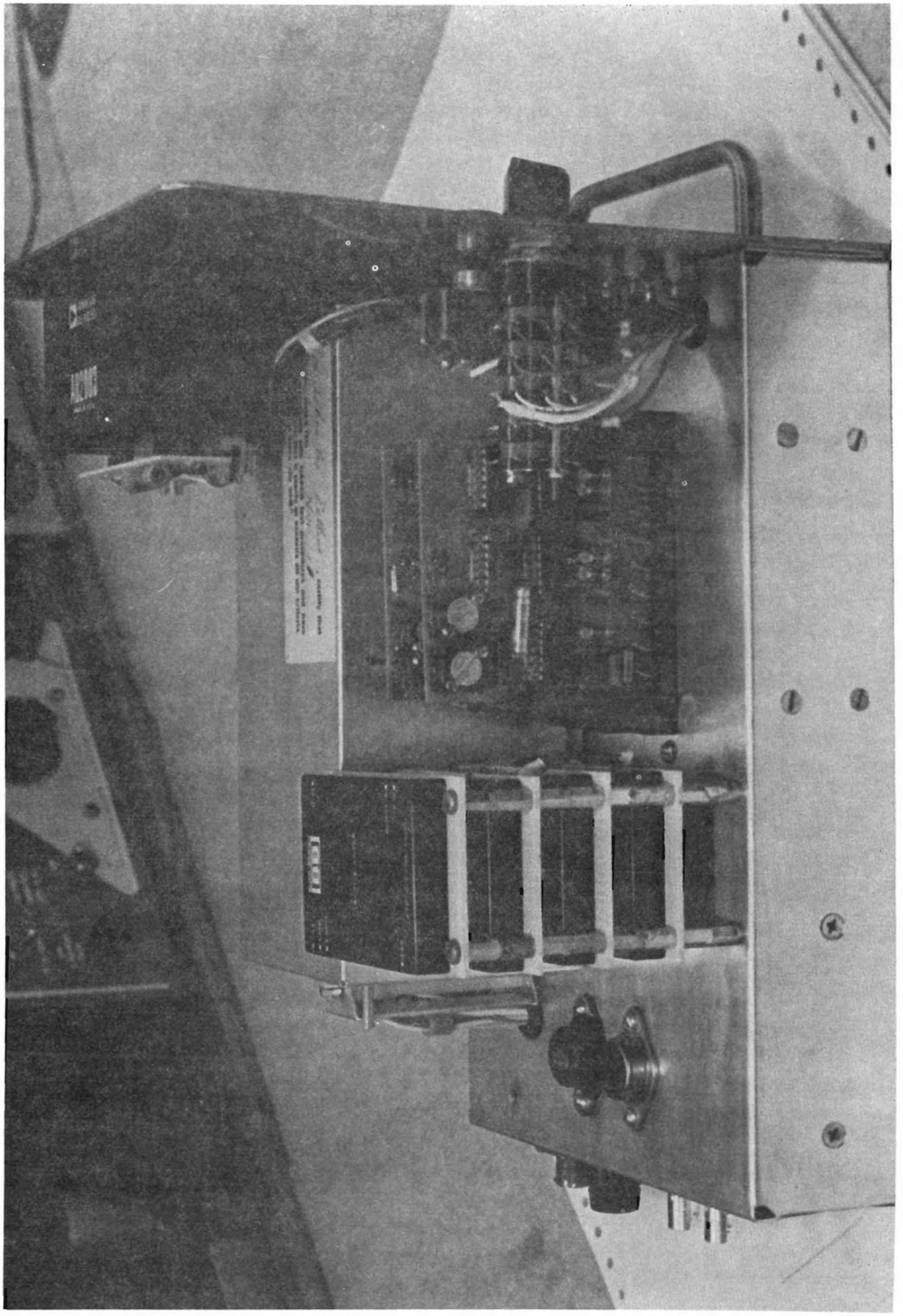

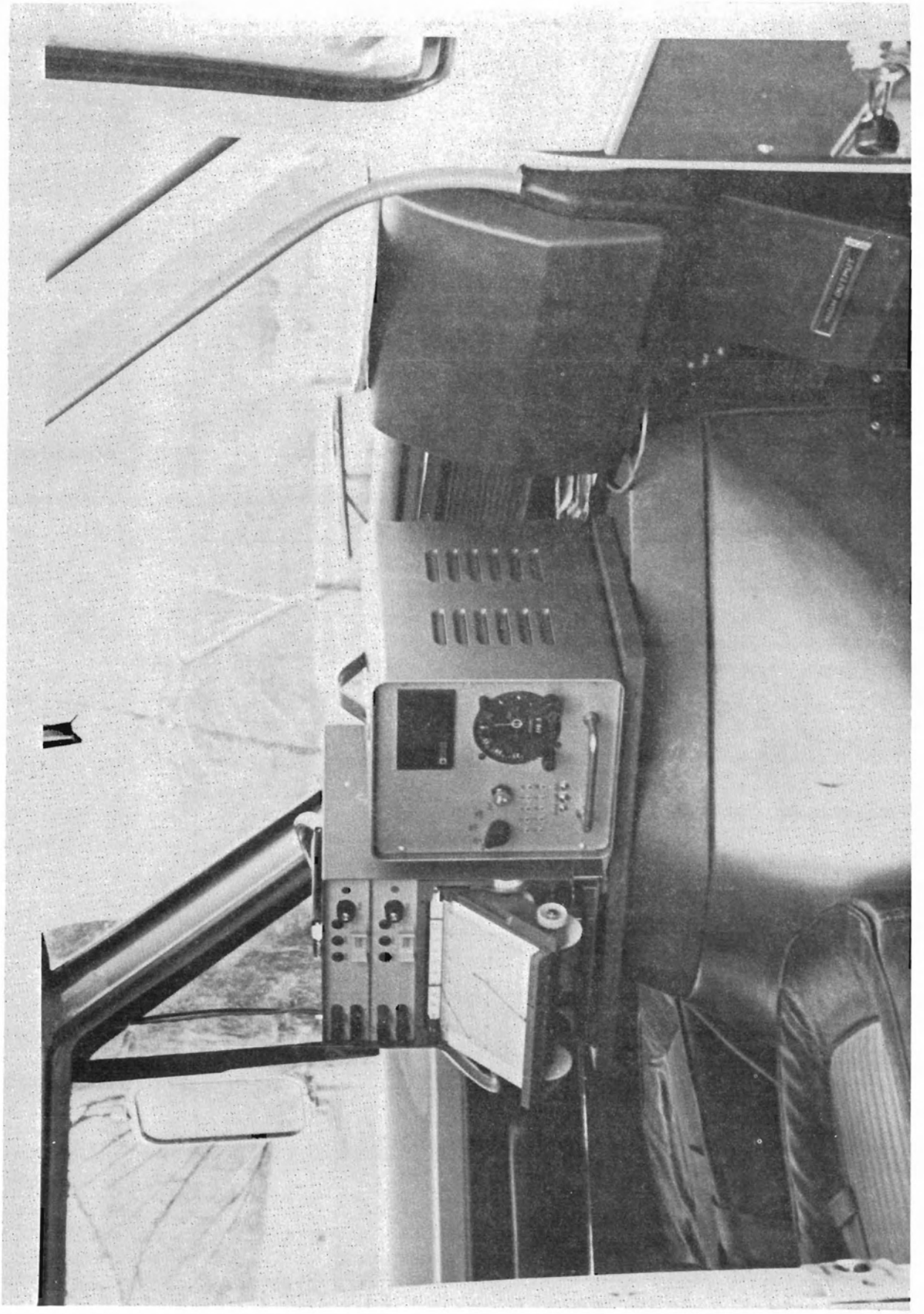

	Linearity	Temperature	Offset	Spurious
Calibrator	0.07%	25 ppm/°C	----	----
Filters	----	25 ppm/°C	----	0.1%
Circuitry	0.1%	25 ppm/°C	----	----
Divider	0.3%	50 ppm/°C	0.1%	----

Table 4.3. Localizer Monitor Error Budget.

The stability and maintenance of these low instrument-error values is largely attributable to the high common-mode signal rejection attendant with the implicit implementation of the DDM calculation. Also, the identical 90 Hz and 150 Hz signal channels and the differential manner in which they are operated upon throughout the monitor. Section B6 discusses these considerations in greater detail.

3. Recommended Improvements. On a short term basis the precision localizer monitor will provide accuracies of 0.33% or 0.00052 DDM. This represents the root-sum-squared linearity error from Table 4.3. This short term accuracy requires a constant temperature environment and sufficient warmup (15 minutes) of the equipment plus a calibration just prior to use. For the prototype model, the practice has been to check the calibration of the monitor against the Boonton calibration test set prior to any actual field use. The stability of the calibrator at present seems better than that obtained from the 90 Hz and 150Hz bandpass filters used in the processor circuitry. No long term calibration data has been obtained as of the release of this report.

As can be seen in Table 4.3, however, the principal difficulty with the prototype mechanization of the precision localizer monitor is temperature sensitivity. Improvement is possible particularly for the active filters. Both the 90 Hz and 150 Hz bandpass filters use stagger-tuned bandpass pole-pairs to realize the required filter shape factor. The difficulty with this method of filter implementation is the sensitivity of the pole position to temperature variations with the Q-values involved. With the prototype localizer monitor, this sensitivity was the principal contribution to a long term DDM drift, for a constant input, on the order of ± 1.5 microamperes. This figure is 3 times the design absolute accuracy value of ±0.5 microampere. A significantly more stable filter mechanization, by half an order of magnitude, has been subsequently designed. In place of a conventional Butterworth bandpass realization, a Chebyshev low-pass filter was synthesized using biquad resonator filter sections whereby the low-pass pole-pairs were transformed to bandpass pole-pairs. This low-sensitivity mechanization exhibits a maximum bandpass variations of 0.1 DB over a temperature range of -20° C to +70° C.

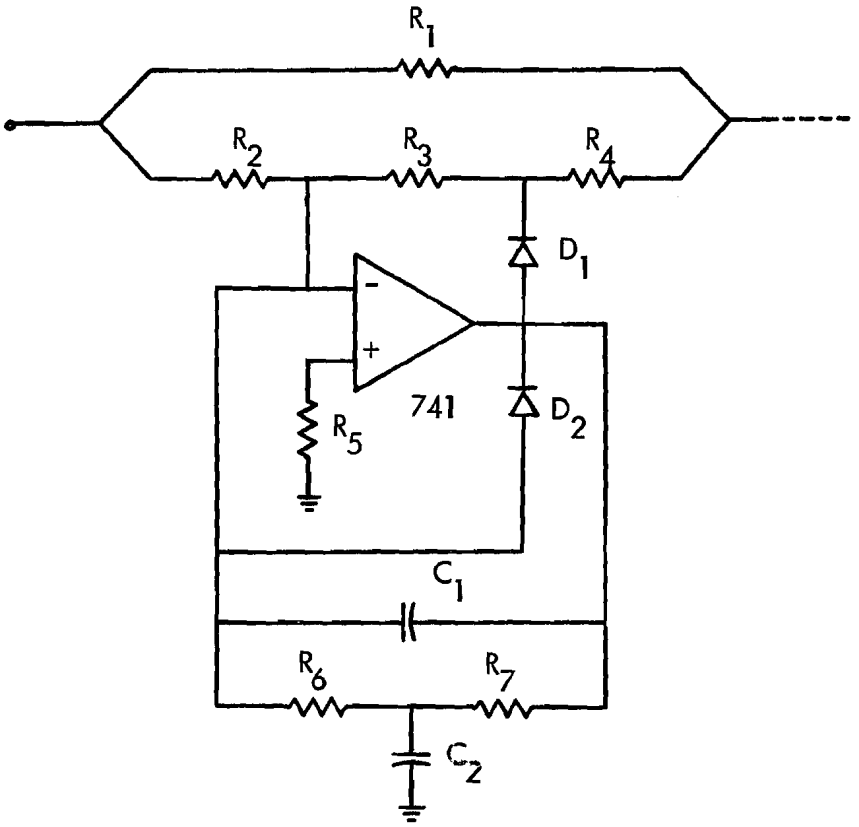

Figure 4-19. Improved Absolute Value Circuit.

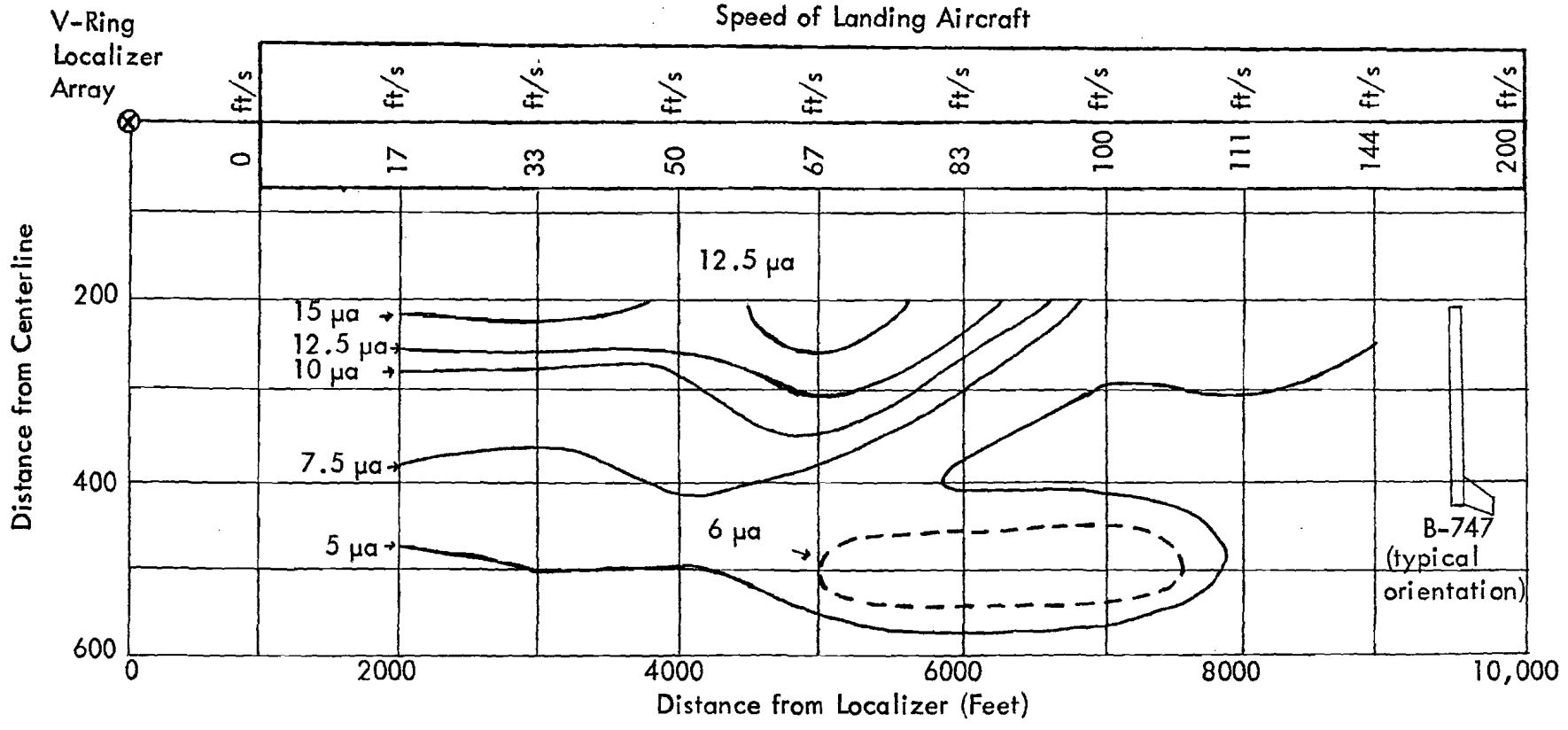

Figure 5-1a. A Contour Map of Peak CDI Response Caused by the Diffraction of Signals by a B-747 Aircraft Parked Perpendicular to the Centerline. Dynamic Response for a Touchdown Speed of 120 Knots.

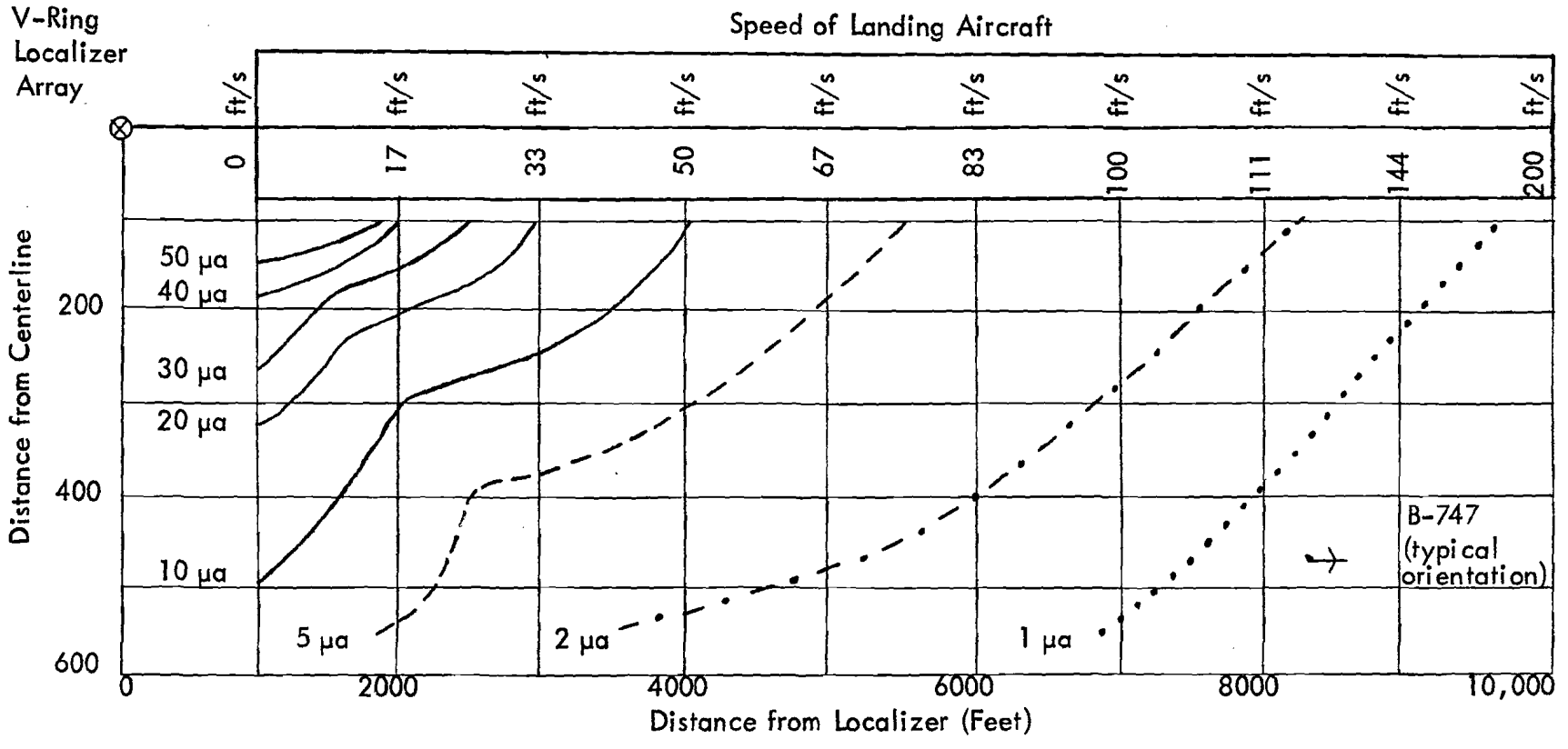

Figure 5-1c. A Contour Map of Peak CDI Current Response Caused by the Reflection of Signals from a B-747 Aircraft Parked Parallel to the Centerline. Dynamic Response for a Touchdown Speed of 120 Knots.

VII. BIBLIOGRAPHY AND REFERENCES

[1] Report No. RD 65-107, Project No. 320-101-01N, "Interference to Aircraft Conducting Category II Instrument Approaches by Other Aircraft in Vicinity of the Airport," October 1965.

[2] SRDS RD 69-18, "An Evaluation of the C-141 Category III All Weather Landing System."

[3] McFarland, Richard, Fred Kiko, G. E. Smith, Report Number FAA-RD-69-44, "VOR Propagation and Stability Study, Final Report," Avionics Research Group, Department of Electrical Engineering, Ohio University, January 1970.

[4] ICAO, AWOP IV-WP/182, 8/9/70, "Measurement of Localizer Course Structure Along Runways."

[5] ICAO, AWOP IV-WP/191, 28/9/70, "Review of Pane's Work on Subject--ILS."

[6] ICAO, AWOP IV-WP/192, 28/9/70, "A Category III ILS Monitoring Concept."

[7] ICAO, AWOP IV-WP/195, 13/10/70, "Specification of Beam Bends for Roll-Out."

[8] SRDS RD 72-71, "Instrument Landing System Improvement Program, Third Interim Report," Contract FA69WA-2066, Avionics Research Group, Department of Electrical Engineering, June 1972.

[9] FAA-RD 72-89, Croswell, Thomas L., "Status of Category III in Europe, Final Report," The MITRE Corporation, Washington Operations, Washington, D. C., June 1972.

[10] International Standards and Recommended Practices, "Aeronautical Telecommunications," Annex 10, Volume 1, Third Edition, July 1972.

[11] SRDS RD-73-137, "Instrument Landing System Improvement Program, Fourth Interim Report," Contract FA69WA-2066, Avionics Research Group, Department of Electrical Engineering, May 1973.

[12] TELS 34/2/069, Reiffer, D.R., "Instrument Landing System for Category III Operation - Multi-path Interference Effects Due to Ground Movement of a Boeing 747 Aircraft on Heathrow Airport, London", January, 1971.

IX. APPENDICES

APPENDIX II. Circuit Modification

Some instability was noted during preliminary use of the prototype Centerline Monitor unit. This instability was traced to the 90 Hz and 150 Hz bandpass filters. In the design (see Figure 4-13a), two filters were used in both the 90 Hz and 150 Hz sections of the circuits, one with a rated Q of 10 and a second with a rated Q of 5, to obtain the design bandpass characteristics of Figure 4-8. Subsequent removal of the lower Q filter from the circuits resulted in improved stability with no noticeable loss in accuracy of the unit. The temperature sensitivity of the prototype monitor, while still not as good as desired, also showed improvement after removal of these filter units.

34695